Therapeutic expression of RAS Degrader RRSP in Pancreatic Cancer via Nanocarrier-mediated mRNA delivery

Taylor E. Escher,[1] Simseok A. Yuk,[2] Yuan Qian,[2] Caleb K. Stubbs,[1] Evan A. Scott,[2,3,4,5] and Karla J.F. Satchell[1,5]

[1]Department of Microbiology-Immunology, Northwestern University, Feinberg School of Medicine, Chicago, IL 60611 United States

[2]Department of Biomedical Engineering, Northwestern University, Evanston, IL 60208, USA.

[3]Simpson Querrey Institute, Northwestern University, Chicago, IL 60611, USA.

[4]Chemistry of Life Processes Institute, Northwestern University, Evanston, IL 60208, USA.

[5]Robert H. Lurie Comprehensive Cancer Research Center, Northwestern University, Feinberg School of Medicine, Chicago, IL 60611 United States

Correspondence should be addressed to:

Karla J. F. Satchell: Northwestern University, Feinberg School of Medicine, Chicago, Illinois, 60611, United States. Email: k-satchell@northwestern.edu; Ph: 312-503-2162

Short title: Nanocarrier delivery of mRNA for RAS degrader

Keywords: RRSP, nanocarriers, RAS, degrader

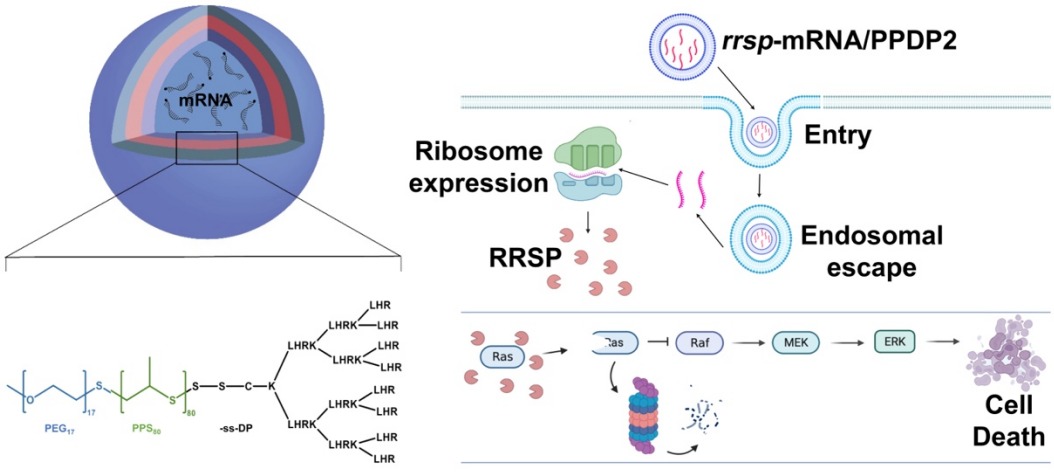

Graphical Abstract: Synthetic nanocarriers packaged with mRNA are used to express the RAS-specific protease RRSP in cancer cells resulting in cell death and tumor shrinkage.

ABSTRACT

About one-third of all human cancers encode abnormal RAS proteins locked in a constitutively activated state to drive malignant transformation and uncontrolled tumor growth. Despite progress in development of small molecules for treatment of mutant KRAS cancers, there is a need for a pan-RAS inhibitor that is effective against all RAS isoforms and variants and that avoids drug resistance. We have previously shown that the naturally occurring bacterial enzyme RAS/RAP1-specific endopeptidase (RRSP) is a potent RAS degrader that can be re-engineered as a biologic therapy to induce regression of colorectal, breast, and pancreatic tumors. Here, we have developed a strategy for in vivo expression of this RAS degrader via mRNA delivery using a synthetic nonviral gene delivery platform composed of the poly(ethylene glycol)-*b*-poly(propylene sulfide) (PEG-*b*-PPS) block copolymer conjugated to a dendritic cationic peptide (PPDP2). Using this strategy, PPDP2 is shown to deliver mRNA to both human and mouse pancreatic cells resulting in RRSP gene expression, activity, and loss of cell proliferation. Further, pancreatic tumors are reduced with residual tumors lacking detectable RAS and phosphorylated ERK. These data support that mRNA-loaded synthetic nanocarrier delivery of a RAS degrader can interrupt the RAS signaling system within pancreatic cancer cells while avoiding side effects during therapy.

INTRODUCTION

Across all stages of pancreatic cancer, the relative survival rate for patients is only 12%. In 2024, this equates to over 50,000 deaths, making it the third most deadly type of cancer in the United States.[1] Oncogenic variants of the Kirsten rat sarcoma (KRAS) protein occur in approximately 95% of patients with pancreatic ductal adenocarcinoma (PDAC). The remaining patients may have wild-type KRAS or mutant variants in neuroblastoma rat sarcoma (NRAS) or Harvey rat sarcoma (HRAS) proteins.[2,3]

In response to growth factors, RAS proteins control cell proliferation in both normal and cancerous cells. Malignant transformation can result in constitutive activation of RAS.[4] RAS has historically been considered “undruggable” as the protein lacks well-defined binding pockets and its GTP-binding site is outcompeted by high concentrations of cellular GTP.[5-8] In addition, multiple *RAS* genes and isoforms are differentially expressed depending on cell type.[4] Currently, Federal Drug Administration (FDA)-approved RAS-directed therapies have focused on targeting specific KRAS mutations, which are only present in a small percentage of all cancers. In addition, clinical use against lung and other cancers has demonstrated these molecules have a high propensity for driving drug-resistance.[9-11] To address these therapeutics gaps, strategies under development

include “RAS Degraders”, which specifically target RAS for proteolytic turnover and result in lowered levels of RAS in the cell that can be useful in treating nearly all tumors. In addition, “pan-RAS” degraders target all forms of RAS in the cell, devoiding cells of RAS and thereby stopping cell proliferation.[12]

In this study, we developed an mRNA-based nanotherapy to express a pan-RAS degrading enzyme within cancer cells to overcome the limitations of current FDA-approved RAS mutant therapies. The RAS/RAP1-specific endopeptidase (RRSP) is a well-studied intracellular RAS Degrader.[12] Originally termed DUF5, RRSP is a bacterial cytotoxic effector domain from the multifunctional-autoprocessing repeats-in-toxin (MARTX) toxin.[13] RRSP site-specifically cleaves RAS and its close homologue RAP1, between residues Tyrosine-32 and Aspartic acid-33 within the Switch I region, thereby preventing interaction with RAF kinases in the RAS-ERK signaling axis. RRSP has been shown to be highly specific and does not target other closely related GTPases.[14,15] RRSP can cleave all three of the major RAS isoforms (H, N, and K), both GTP and GDP-bound RAS, as well as the most common oncogenic RAS mutations, including G12C, G12D, G12V, G13D, and Q61R.[14-16] Within cells, RRSP degradation of RAS leads to G1 cell cycle arrest that can progress to apoptosis, senescence, and loss of cell proliferation in more than 80% of all cells lines where it has been tested, including leukemia, non-small cell lung carcinoma, colorectal carcinoma, central nervous system cancers, melanoma, ovarian cancers, renal cancers, pancreatic cancer, and breast cancer.[13,16-18]

The major limitations to use of RRSP as a cancer therapeutic are its size (56 kilodaltons (kDa)) and that the active domain cannot transit across the cell plasma membrane without the remaining portions of the larger toxin. The advent of nucleic acid delivery to cells using synthetic nanocarriers provides a key strategy for RRSP to be expressed within cells for RAS degradation and loss of cell proliferation.[19,20] Previous studies established that RRSP could be expressed in cells following transfection of plasmids with the primary genetic sequence for RRSP cloned under the control of eukaryotic expression promoter, with the expression of RRSP resulting in cytotoxicity.[13] In addition, lipid nanoparticles (LNPs) have been used to deliver *rrsp*-mRNA to colon cancer cells, which induced cell cytotoxicity, cleavage of RAS, and reduction of tumors.[21] Here we tested a nonviral synthetic delivery platform composed of the self-assembling polymer poly(ethylene glycol)-*b*-poly(propylene sulfide) (PEG-*b*-PPS) conjugated to a dendritic cationic peptide (PPDP2)[20]. We have demonstrated that delivery of an RRSP encoding *rrsp*-mRNA via PPDP2 achieves rapid intracellular degradation of RAS. In addition, PPDP2 can deliver RRSP-encoding

mRNA to cells in culture or within tumors in vivo. Following delivery by PPDP2, RRSP is highly expressed, cleaves RAS, and leads to cell death and tumor regression.

RESULTS

PPDP2 synthetic nanocarriers deliver mRNA for expression in cancer cells and tumors.

Efficient and scalable methods have been described for loading bioactive molecules within PEG-*b*-PPS synthetic nanocarriers.[22,23] PEG-*b*-PPS synthetic nanocarriers have been tested across diverse disease models,[19,24,25] and validated as non-immunogenic in human blood.[26] The platform has been demonstrated not to induce an inflammatory response and is non-toxic in non-human primates,[23] and humanized mice.[11] The platform was recently engineered for delivery of nucleic acids by linking a cationic DP via a reduceable bond to generate the synthetic nanocarrier PPDP2 (Figure 1A).[20] PPDP2 undergoes pH-dependent disorder-to-order transitions to adopt a unique helical conformation under acidic conditions that promotes the cytoplasmic release of diverse payloads intracellularly.[20] The optimized nanocarrier construct has low toxicity, regardless of cargo size, and transfects under standard culture conditions in the presence of serum.[20]

While PPDP2 has demonstrated efficient packaging and delivery of DNA plasmids[20], it had not been previously employed for mRNA transfection. For this study, our first objective was therefore to test whether PPDP2 nanocarriers would deliver mRNA into nonphagocytic cancer cells. In human pancreatic PANC-1 cells, PPDP2 nanocarriers demonstrated successful delivery of *egfp*-mRNA (1 μg) to cancer cells resulting in GFP expression (Figure 1B). The number of GFP-positive cells was highly efficient, with ~80% of cells transfected. The efficiency of transfection was 2.5-fold higher than cells treated with *egfp*-mRNA alone and was similar to transfection of *egfp*-mRNA using MessengerMAX lipofectamine (Figure 1C). Successful delivery was also demonstrated in KPC mouse pancreatic cells (Figure S1). These data support that PPDP2 synthetic nanocarriers can be used for the delivery of mRNA resulting in expression of protein in nonphagocytic cancer cells.

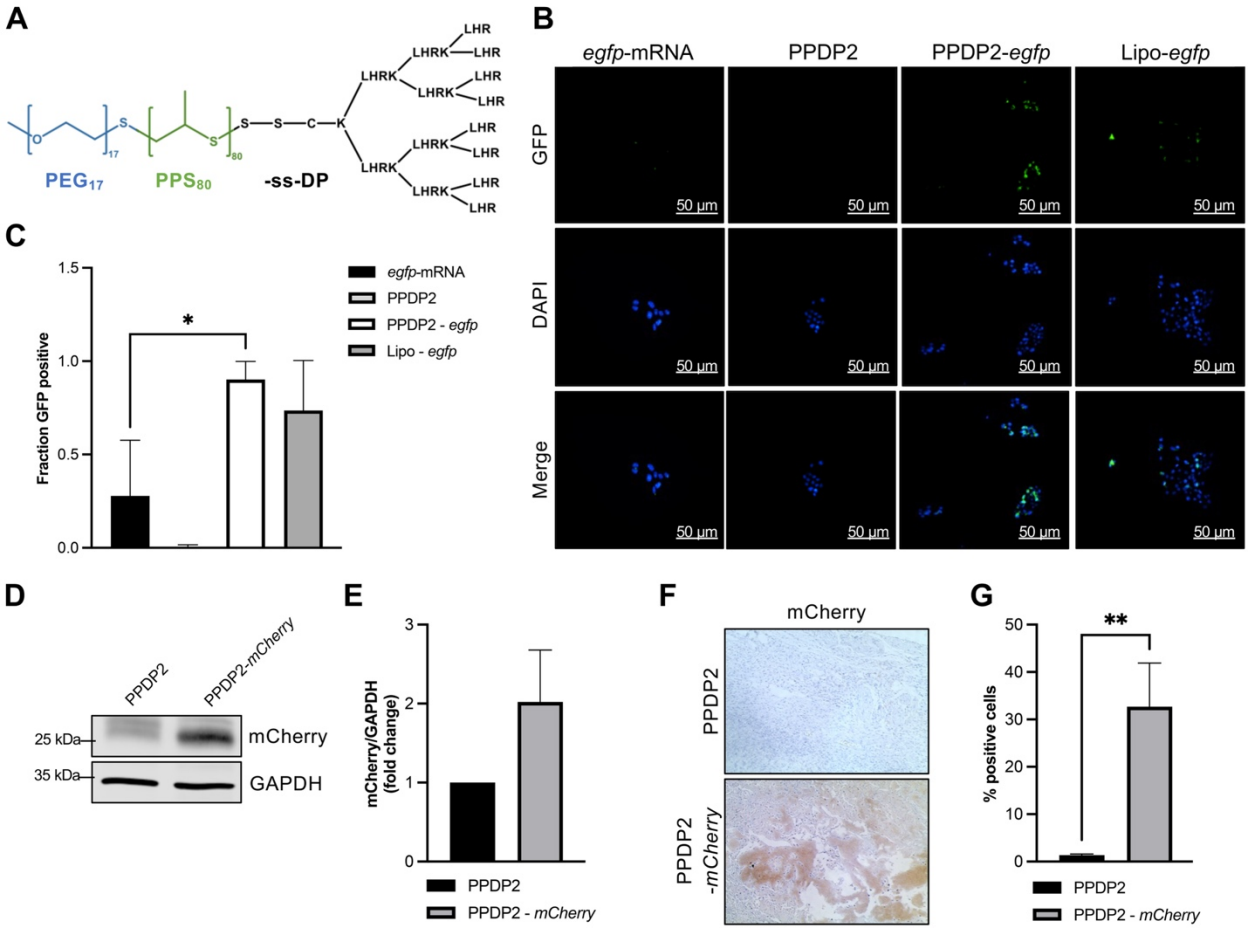

Figure 1. PPDP2 nanocarriers deliver *egfp*-mRNA and *mCherry*-mRNA into pancreatic cancer cells (A) Schematic of nanocarrier chemistry. **(B)** Representative fluorescent images of PANC-1 cells after transfection of cells with 1 µg of *egfp*-mRNA alone, PPDP2 alone (1:40 w/v%) (PPDP2), *egfp*-mRNA (1 µg) with PPDP2 (PPDP2-*egfp*) or *egfp*-mRNA (1 µg) with MessengerMAX Lipofectamine (Lipo-*egfp*). **(C)** Quantification of the fraction of GFP positive cells (green) from five imaged frames are shown as a histogram. **(D)** Representative Western blot and (**E**) quantification of mCherry levels from PANC-1 xenografts injected with PPDP2 alone (PPDP2) or PPDP2–*mCherry*-mRNA (PPDP2-*mCherry*) (n=3). **(F)** mCherry IHC staining and (**G**) quantification from PANC-1 xenografts injected as indicated (*n*=4). P values were calculated using a one-way ANOVA and Dunnett's multiple comparisons test, **p*<0.05, ***p*<0.01

To assess expression of protein in tumors following PPDP2 synthetic nanocarrier delivery of mRNA, we tested *mCherry*-mRNA delivery by PPDP2 into xenograft tumors. PANC-1 pancreatic cell-based xenograft (CBX) tumors were first established in immunodeficient *nu/nu* mice and then tumors were treated by intratumoral (i.t.) injection with PPDP2/*mCherry*-mRNA. After four weeks of treatment three times per week (excluding weekends), resected tumors showed high levels of expression of mCherry by Western blotting (Figure 1D,E) and by immunohistochemistry (IHC) staining (Figure 1F,G).

Altogether, these data support that mRNA delivered with PPDP2 can result in protein expression within non-phagocytic cells and within tumors. These results support that PPDP2 delivery of mRNA could be an effective strategy for anti-tumor therapy.

PPDP2-*rrsp*-mRNA reduces levels of RAS and impacts cell proliferation in pancreatic cancer cells.

Next, we sought to determine whether we could employ PPDP2 synthetic nanocarriers for delivery of *rrsp*-mRNA for expression of the RRSP RAS degrader within cells. As a preliminary assessment, we established first that synthetic produced *rrsp*-mRNA would serve as a template for protein production and impact cell proliferation. To match prior studies,[16] HCT-116 colon cancer cells were transfected with mRNA mixed with MessengerMAX lipofectamine for 24 hours and treated with *egfp*-mRNA or rrsp-mRNA (Figure S2A,B). Cells treated with control *egfp*-mRNA were normal in appearance and produced EGFP while *rrsp*-mRNA treated cells showed cytotoxicity and changes to cell morphology (Figure S2B). Even at concentrations as low as 0.5 µg, expression of RRSP from the mRNA resulted in loss of detectable RAS in cell lysates using a pan-RAS antibody (Figure S2C). Similar studies in mouse KPC pancreatic cells showed that transfection with *rrsp*-mRNA and lipofectamine resulted in loss of cell proliferation and reduced confluency (Figure S3A,B).

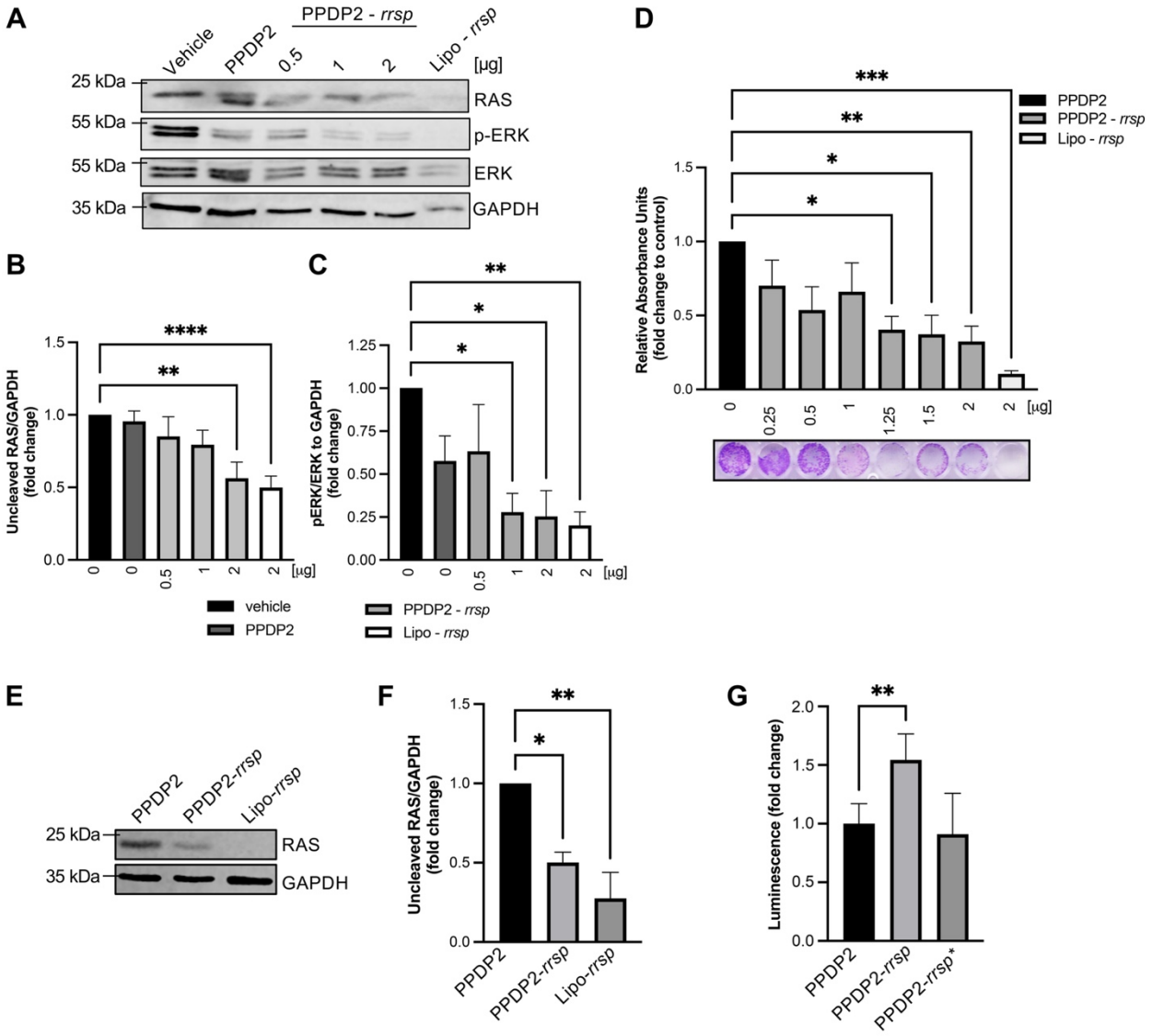

Figure 2. PPDP2-*rrsp*-mRNA reduces levels of RAS and impacts cell proliferation in human pancreatic cancer cells. (A) Representative Western blot of RAS and pERK levels of PANC-1 cells transfected for 24 h with either vehicle only, PPDP2, PPDP2 nanocarriers loaded with *rrsp*-mRNA (PPDP2-*rrsp*) or *rrsp*-mRNA mixed with MessengerMAX lipofectamine (Lipo-*rrsp*) as indicated. **(B,C)** Densitometry quantification from replicate Western blots for RAS and phospho-ERK (*n*=5). **(D)** Spectrophotometer quantification (*n*=3) and representative image of crystal violet-stained colonies from PANC-1 cells treated as indicated in legend. **(E,F)** Representative Western blot and densitometry quantification (*n*=3) of uncleaved/cleaved RAS levels of PANC-1 cells after 24 treatment with 5.5 µg PPDP2-*rrsp*-mRNA, indicative of dose for following mouse experiments. **(G)** Caspase Glo 3/7 luminescence activity of PANC-1 cells treated with PPDP2 and 5.5 µg rrsp-mRNA (PPDP2-*rrsp*) or catalytically inactive rrsp*-mRNA (PPDP2-*rrsp**) (*n*=5). Data are

presented as mean ± SEM. P values were calculated using a one-way ANOVA and Dunnett's multiple comparisons test, * $p < 0.05$, ** $p < 0.01$, *** $p < 0.001$.

As a further test to demonstrate relevance to pancreatic cancer and to benchmark transfection using PPDP2, human pancreatic PANC-1 cells were treated with varying concentrations of *rrsp*-mRNA using either PPDP2 or lipofectamine. After 24 h, we found a significant 40% reduction in total levels of RAS in cells treated with 2 µg *rrsp*-mRNA using both PPDP2 and lipofectamine as the delivery method for *rrsp*-mRNA (Figure 2A,B). Phospho-ERK expression was also significantly reduced, indicative of RRSP inhibiting the downstream RAS signaling pathway (Figure 2A and 2C). Further, as low as 1.25 µg of *rrsp*-mRNA delivered by PPDP2 in PANC-1 cells showed significant reduction (over 60%) in cell proliferation measured by crystal violet staining (Figure 2D). Increasing to 5.5 µg showed loss of all RAS in cells (Figure 2E,F). In addition, caspase-3/7 Glo assays demonstrated an increase in caspase activity following treatment with 5.5 µg *rrsp*-mRNA. This effect was not seen when mRNA that encodes for catalytically inactive RRSP was transfected, demonstrating that caspases were activated specifically in response to RAS cleavage (Figure 2G). These experiments were replicated in KPC cells demonstrating that *rrsp*-mRNA is effective in reducing RAS when delivered by PPDP2 synthetic nanocarriers. PPDP2 resulted in slightly, although not significantly, improved *in vitro* efficiency compared to lipofectamine (Figure S4A-D).

PPDP2-*rrsp*-mRNA reduces pancreatic tumor growth by reducing RAS and phospho-ERK levels.

Since PPDP2-*rrsp*-mRNA reduced cell proliferation *in vitro* in pancreatic cells and we have previously shown that RRSP-DT_B causes PDAC tumor regression[17,18], we next asked whether PPDP2-*rrsp*-mRNA affects PDAC tumor xenograft growth in mice. For these studies, the *rrsp*-mRNA is identical to that used for cell-based studies except that sequences for a hemagglutinin tag were added for antibody detection of the protein expressed in tumors. In addition, an *rrsp**-mRNA that expresses the H451A mutant, and thus cannot cleave RAS, was added as an additional control. PANC-1 xenograft tumors were established and then treated by i.t. injection with PPDP2 alone, PPDP2-*rrsp*-mRNA, or PPDP2-*rrsp**-mRNA at a dose of 0.25 mg mRNA/mouse kg dose, which is equivalent to 5.5 µg mRNA in cellular studies (Figure 2E-G). While tumors continued to grow in the PPDP2 alone group, there was a significant reduction in tumor size in both treatment groups with 70-80% reduced growth after treatment with *rrsp*-mRNA and 50-60% after treatment with *rrsp**-mRNA (Figure 3A-E). There was no change in mouse

weight over the course of the experiment indicating no generalized toxicity (Figure 3F). Two representative tumors treated with PPDP2-*rrsp*-mRNA showed high expression of RRSP in tumor tissue (Figure S5A,B). The management of tumor growth by delivery of the *rrsp**-mRNA was surprising. This result suggests that the expression level of RRSP* is sufficiently high in tumor cells to bind Switch 1 and block RAF association and/or exchange of GDP for GTP, preventing the generation of active RAS without enzymatic cleavage.

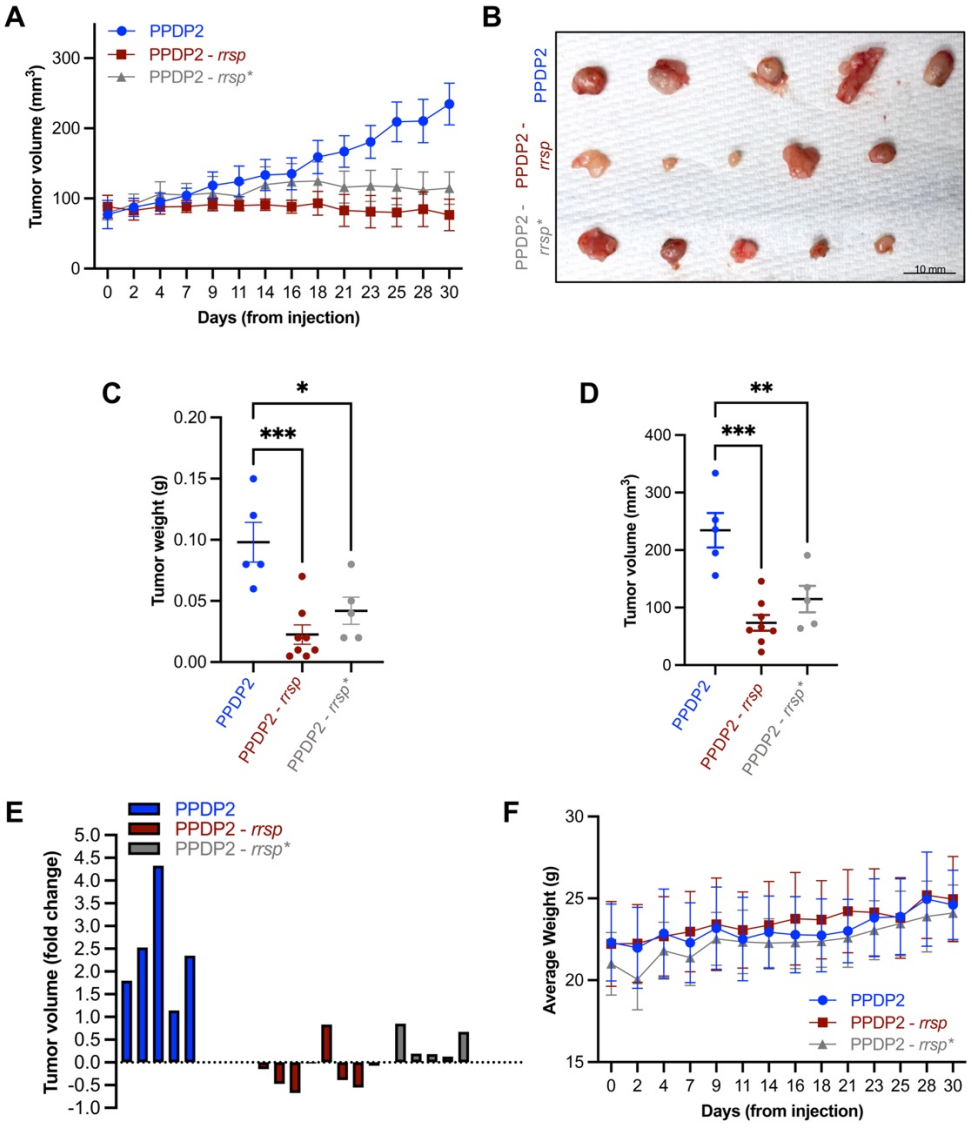

Figure 3. PPDP2-*rrsp*-mRNA inhibits growth of pancreatic tumors. (A) PANC-1 xenograft tumors were established and tumor volume measured every other day, excluding weekends. Day 0 indicates day of first treatment with 0.25 mg/kg dose of PPDP2-*rrsp*-mRNA (red) three times per week compared to PPDP2-*rrsp**-mRNA (grey) or PPDP2 alone (blue). **(B)** Images of

resected tumors on Day 30. **(C)** Tumor weight, **(D)** tumor volume and **(E)** change in volume compared to first day of treatment, normalized to 0, on Day 30. **(F)** Weight of mice measured every other day. Data were presented as mean ± SEM with $n = 5$. P values were calculated using a one-way ANOVA and Dunnett's multiple comparisons test, * $p < 0.05$, ** $p < 0.01$, *** $p < 0.001$.

Tissue staining showed control PANC-1 tumors treated with only PPDP2 had enlarged nuclei and cytoplasm with dense collagen layers (Figure 4A), along with high expression level of the CK-19 cytokeratin marker indicative of PDAC (Figure 4B) and of the Ki-67 proliferation marker (Figure 4C). Both RAS and phospho-ERK levels were high, consistent with active tumor growth (Figure 4D,E). By contrast, tumors treated with PPDP2-*rrsp*-mRNA showed reduced cell cytoplasm, immune cell infiltration, and loss of tumor tissue density or organization (Figure 4A). CK-19 and Ki-67 levels were reduced or absent (Figure 4B,C). Most notably, RAS and phospho-ERK levels were significantly reduced, which is indicative of target engagement (Figure 4D,E). Notably the PPDP2-*rrsp**-mRNA group did not show reduced RAS levels (Figure 4D), which is consistent with the expressed RRSP* protein not being able to cleave RAS. There was however a statistically significant loss of phospho-ERK in tumor tissue following treatment with *rrsp**-mRNA (Figure 4E), consistent with the suggestion that catalytically inactive RRSP* may be binding to RAS and inhibiting its downstream effect on ERK. Overall, our data show that both *rrsp*-mRNA and *rrsp**-mRNA delivered through PPDP2 nanocarriers significantly inhibit RAS signaling albeit by different mechanisms, both resulting in tumor regression.

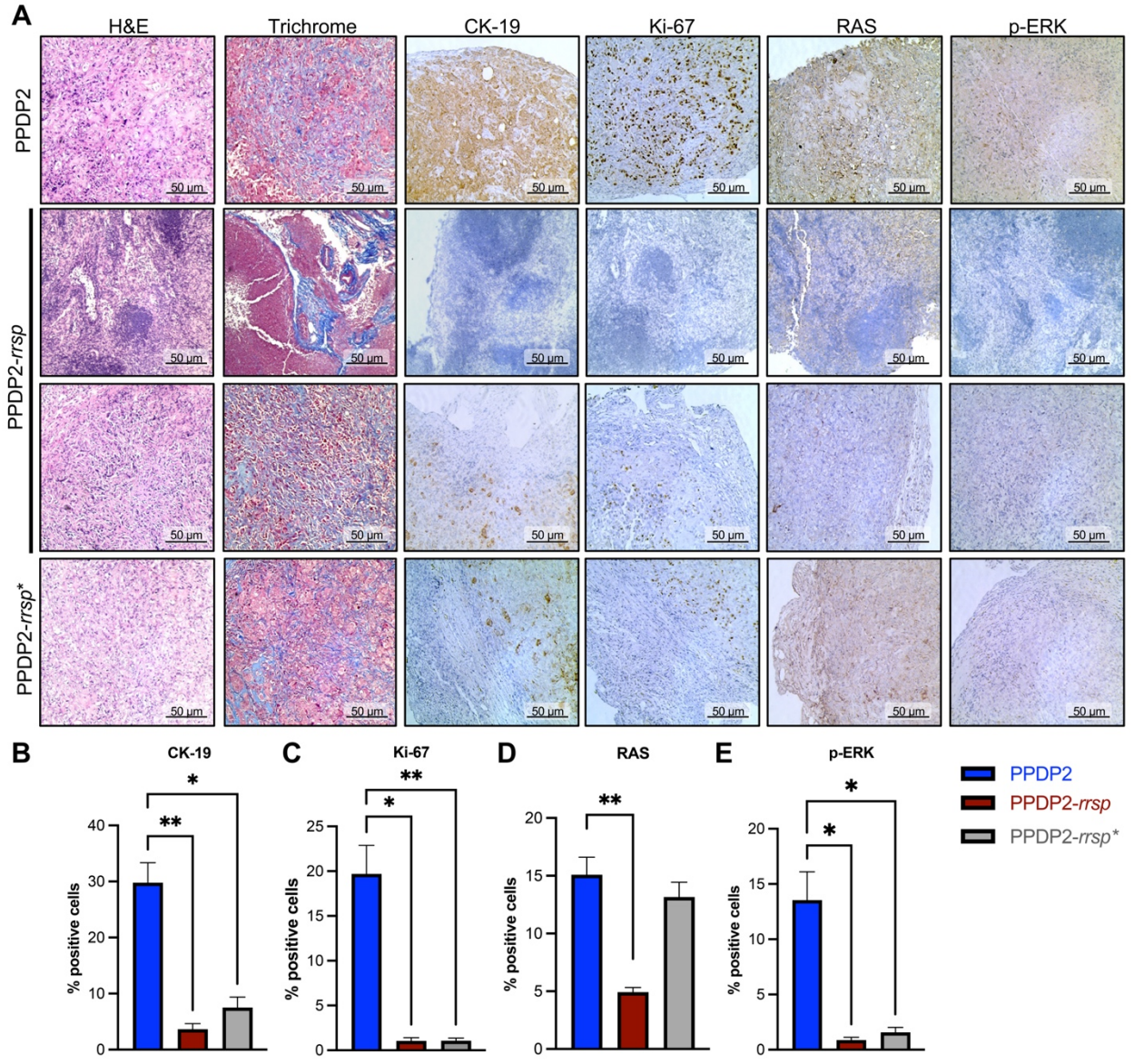

Figure 4. PPDP2-*rrsp*-mRNA impact on tissue organization and protein expression. (A) H&E, Masson's trichrome, and IHC staining with anti-CK-19, anti-Ki-67, anti-pan-RAS, and anti-phospho-p44/42 MAPK. **(B-E)** ImageJ was used to quantify intensity of brown staining as indicated at top (*n*=5). Data were presented as mean ± SEM. *P* values were calculated using a one-way ANOVA and Dunnett's multiple comparisons test, assuming equal distribution * $p < 0.05$, ** $p < 0.01$.

In a replicate experiment, tumors were grafted to both flanks of *nu/nu* mice, but only the primary tumor was treated with PPDP2-*rrsp*-mRNA while the secondary tumor on the opposite flank was not treated. The treated tumors regressed as seen in the first experiment (Figure S6A). The

PPDP2 control tumors in the treated flank (Figure S6A) as well as all of the untreated secondary tumors on the untreated flank (Figure S6B) did not regress and grew at similar rates to the PPDP2 treatment group. Following cessation of treatment at day 22, mice were kept without treatment for another 25 days. The treatment group did not show growth of resistant tumors while tumors in the control groups and non-treated secondary tumors showed slight growth (Figure S6A,B). Mice in all groups did not show significant weight loss (Figure S6C). This experiment indicates that treatment of one flank does not result in reduction of tumors on the opposite flank.

Systemic delivery of RRSP exhibits low toxicity in DTR knock-in mice.

For future pre-clinical development, it may be necessary for systemic delivery so we sought to explore if generalized toxicity of systemic RAS inhibition would occur if RRSP was systemically delivered. We previously showed that intraperitoneal delivery of RRSP-DT_B can reduce tumors when specifically targeted to human cells, as mice lack a high affinity receptor for DT_B.[17,18] Herein, we explored the level of toxicity if the protein was accessible to all cells in the mouse. For this experiment, we created diphtheria toxin receptor (DTR) knock-in mice, expressing the high affinity human diphtheria toxin receptor HB-EGF in all cells, with the assistance of Jackson Laboratory. The DTR knock-in mice were treated intraperitoneally with various doses up to 0.5 mg/kg of RRSP-DT_B.[27] or catalytically inactive RRSP*-DT_B three times per week for 4 weeks. Mouse weights and general health were monitored, and deaths recorded (Figure S7A). In the 0.5 mg/kg group, 3 mice died, and one mouse died from the 0.25 mg/kg group. No other deaths occurred, and mouse weights remained stable or increased throughout the experiment (Figure S7B). Overall, we found the maximum tolerated dose to be 0.25 mg/kg of RRSP-DT_B when delivered systemically to all accessible cells, which is the same value previously found for mice without the transgene where RRSP-DT_B is targeted to only human cells.[17] Necropsy showed the treated mice without any significant changes to tissue architecture within the major organs (Figure S7C). Upon termination of the experiment, we validated the presence of DTR in the peripheral blood mononuclear cells (PBMC) compared to DTR WT mice by Western blot (Figure S7D) and by flow cytometry (Figure S7E). Overall, these data suggest that systemic inhibition of all RAS is not toxic to mice, likely as RAS is only functional in actively growing cells.

Structural modeling of RRSP/RAS indicates low risk of resistance.

A major concern currently for RAS-directed therapeutics is the development of resistance by gain of additional mutations in RAS[12] or increased expression of other RAS proteins such as MRAS.[28] A major asset for RRSP is that it is a pan-RAS inhibitor that targets all isoforms of RAS, so resistance is less likely to emerge by upregulation of a rare form of RAS unless the isoform gained a mutation that would resist binding of RRSP. Following 25 days of no treatment, the residual tumors treated with *rrsp*-mRNA showed no regrowth (Figure S6). Similar findings were previously found for pancreatic tumors treated with RRSP-DT_B.[17]

To consider further the likelihood of RRSP resistant RAS mutations to arise, we generated an AlphaFold2 (AF2) model of the dimeric structure of RRSP bound to KRAS (Figure 6A). RRSP is a multidomain protein with a membrane targeting N-terminal domain C1 and a large C-terminal C2 domain formed as two lobes (termed C2A and C2B) joined by a long flexible helix. An initial analysis revealed that the RRSP membrane targeting C1 domain does not form contacts with RRSP (Table S1) consistent with removal of C1 not impacting cytotoxicity of RRSP.[13] The AF2 model predicts that the C2 domain does bind with RAS with close contact (defined as <4 angstrom) at 26 distinct residues of the RAS G-domain (Table S1 and Figure 6B,C). Residues 21-35 comprising the Switch 1 and neighboring residues are inserted into the active site of the C2B lobe with catalytic residues directed toward the scissile bond. However, unexpectedly, the majority of contacts between RAS and RRSP are not between the C2B catalytic lobe and the Switch 1 of KRAS. The primary site of recognition of KRAS is formed by the RAS β-sheet (β1-β2-β3) as well as with helix α2. This AF2 model is supported by prior data that overexpression of C2A alone in cells is cytotoxic, whereas overexpression of C2B alone is not cytotoxic in the absence of C2A.[13] Hence the high specificity of RRSP for RAS is dictated outside of the Switch 1, even though there is sequence specificity for cleavage of the RAS Switch 1.[15] Further, the residues of theβ-sheet that contact RRSP are conserved across all RAS molecules, as well as RAP1 (Figure 5D). This very large area of contact sites suggests that a single mutation in RAS would not impede susceptibility of the molecule. Thus, the modeling supports that gain of additional mutations in RAS are unlikely to lead to resistance as any

single point of contact is not likely essential and multiple mutations would be required for resistance. Indeed, one direct contact residue is Q61 in Switch 2 although a Q61R mutation remains susceptible to RRSP.[13] Also, any single mutation in the Switch 1 did not impact susceptibility to RRSP.[15] Thus, protein modeling supports our finding that RRSP is not likely to result in resistance from emergence of a KRAS mutation and as all RAS isoforms are cleaved in the cell.

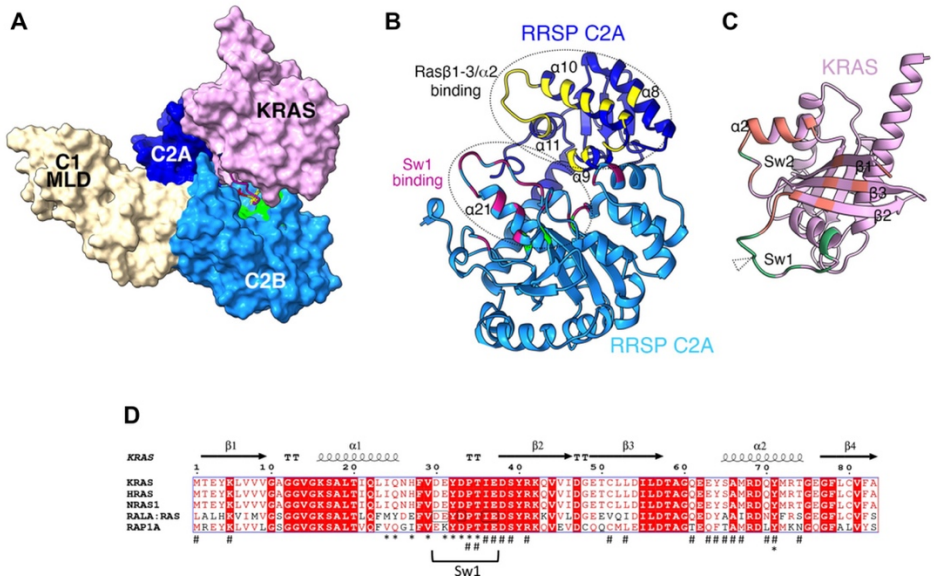

Figure 5. Structural model of RRSP in complex with KRAS suggests extensive contact sites. (A) Space filling AlphaFold2-generated model of RRSP (MARTX toxin aa 3594 – 4078) in complex with KRAS (aa 1-175). RRSP C1 membrane localization domain (MLD, white), C2A (dark blue), C2B (medium blue), and KRAS (pink). Switch 1 (Sw1) is shown only as a ribbon in magenta with D32 and Y33 as sticks in yellow. Catalytic residues are colored lime green. Note that the Sw1 is pulled into the active site of RRSP. **(B)** Ribbon cartoon of RRSP (with C1 MLD removed) with backbone colored as in Panel A. Residues mapped as binding to KRAS are colored (residues that bind C2A are yellow and that bind C2B are magenta) **(C)** Residues in KRAS mapped as binding to C2A are colored orange and to C2B are colored green. Scissile bond is marked with triangle. **(D)** Alignment of all RAS sequences experimentally validated as successfully cleaved by RRSP. RALA:RAS is a chimera with 4 aa changes that alters the noncleaved RalA Sw1 to match the KRAS Sw1 (changed residues outlined) and is cleaved with equal efficiency

as KRAS. 27 residues mapped as binding RRSP C2A are indicated with a hashtag (#) and to RRSP C2B as an asterisk (*). Sw1 and Sw2 are marked in panels C and D.

DISCUSSION

Uncontrolled mutant KRAS signaling drives the onset and progression of 95% of pancreatic cancers.[29] Although many mutant KRAS inhibitors exist, none are currently approved for use in PDAC.[12] Recently, Sotorasib, a KRAS G12C inhibitor, has shown clinical activity in heavily pretreated patients with KRAS G12C-mutated metastatic pancreatic cancer.[30] However, KRAS G12C mutations are only present in 1-2% of PDAC cases. Therefore, a need exists for a pan-RAS inhibitor that is effective against all RAS isoforms and variants and that avoids drug resistance.

Originally termed DUF5, RRSP is a bacterial cytotoxic effector domain from the MARTX toxin.[14] RRSP is a pan-RAS protease with high binding specificity for the RAS core and site-specific processing within the Switch I region. RRSP cleaves all three major RAS isoforms (H-/N-/K-RAS) and the common oncogenic RAS mutants.[13-16] Previously we engineered a proposed biologic therapeutic RRSP-DT_B, for treatment of tumors.[18] We showed that RRSP-DT_B can inhibit cell growth and proliferation at picomolar concentrations of many cell lines, including breast, colorectal, and PDAC cells.[16-18] We showed RRSP-DT_B can slow growth or cause regression of triple-negative breast and colon cancer xenografts as well as pancreatic cancer.[17] In this study we adopt an alternative approach for tumor therapy with RRSP by employing a nonviral synthetic mRNA delivery platform to express a pan-RAS degrading enzyme within cancer cells. This method has an advantage that RRSP is expressed within cells, avoiding complications associated with recombinant protein production, purification, and intracellular delivery.

The PEG-*b*-PPS derivative PPDP2 was specifically developed for delivery of large plasmids to innate and adaptive immune cells.[20] Our data herein demonstrate that PPDP2 can also deliver mRNA to nonphagocytic cancer cells and tumors, resulting in expression of fluorescent proteins GFP and mCherry. Further, delivery of *rrsp*-mRNA via PPDP2 achieved rapid intracellular degradation of RAS in both human and mouse PDAC cells and inhibited pancreatic tumor growth. Compared to other gene delivery vehicles, PPDP2 demonstrated a remarkable ability to achieve these results with no detectable toxicity despite four weeks of administration every other day, which was demonstrated by no weight loss or signs of distress in the animals.

Of note, this study was likely conducted with more PPDP2 and/or mRNA than necessary, as evidenced by the high expression levels of both mCherry and RRSP proteins. Indeed, the expression of inactive RRSP* was sufficient to inhibit tumor growth, which is likely due to RRSP blocking RAS activity via high concentration binding of RAS, as opposed to enzymatic cleavage. The binding affinity of RRSP for KRAS is in the high micromolar range.[31] AF2 modeling for this study shows that the noncatalytic C2A domain of RRSP is a major contact site for KRAS, and we previously found that overexpression of C2A alone is sufficient for cytotoxicity.[13] Thus, our data support that advanced pre-clinical studies to determine optimal dosing via the i.t. route of delivery would be advantageous to determine if less material is needed to achieve to tumor reduction.

In advance of further studies using alternative delivery routes beyond i.t. injection, we explored whether cleavage of RAS would be toxic to animals if RRSP was delivered systemically. Supplemental data show that when RRSP has systemic access in mice, the animals showed the same 0.25 mg/kg maximum tolerable dose as when targeted solely to human cancer xenograft.[18] These published data demonstrate that RRSP may be safe even without cancer cell-specific targeting. These results are supported by recent reports from Revolution Medicine that their anti-pan-RAS small molecule therapeutic is effective, safe, and tolerated in humans.[32]

Recently, another group has tested delivery of *rrsp*-mRNA using LNPs optimized for activity in the higher reactive oxygen species tumor microenvironment.[21] Our delivery system does not need this specific environment for payload release. Of note, our PPDP2 platform has substantial advantages with respect to scalability, safety, and versatility compared to LNPs. PEG-*b*-PPS nanocarriers have been validated as stable delivery vehicles for targeting diverse therapeutics to specific cells and tissues in a wide range of preclinical animal disease models,[11,20,33,34] including in nonhuman primates.[23] PEG-*b*-PPS is nontoxic in mice and nonhuman primates up to 200 mg/kg,[23] and the polymer is amenable to industrial scale production at comparatively low cost.[22,35] The recently engineered PPDP2 derivative forms a stable complexation with nucleic acids for nontoxic gene delivery and long-term storage.[20,36] The triblock copolymer is soluble in water, allowing simple mixing with nucleic acid solutions to initiate assembly into monodisperse vesicles consisting of a PEG exterior, PPS membrane, and dendritic peptide/nucleic acid complex interior lumen. A loading efficiency over 99% for plasmids has been demonstrated.[20] Importantly, the dense PEG exterior prevents interactions between the cationic block with cell membranes and nonspecific serum proteins, allowing nontoxic transfection and maintaining stability under diverse solution conditions. This nontoxic transfection combined with the stability of the PPS membrane

makes PPDP2 well suited for *in vivo* applications. Our work presented here verifies that these prior findings for plasmid delivery also hold true for mRNA payloads, highlighting the versatility of the PPDP2 platform for nucleic acid delivery in general.

The final concern for implementation of a RAS-directed therapy is the potential for emergent resistance. Resistance to small molecule RAS-inhibitors are driven in part by chemistries directed to only mutant RAS, allowing for resistance to emerge from amplification or gain of activating mutation in other RAS isoforms.[37-41] The pan-RAS nature of RRSP reduces the likelihood of resistance by upregulation of alternative non-targeted RAS proteins or by mutations that avoid interaction of RAS with RRSP. A further advantage of naturally occurring toxins, as opposed to laboratory-evolved enzymes, is that they benefit from millions of years of natural selection to have exquisite and multifaceted interaction with their target proteins. As RRSP has nearly 30 points of contact with KRAS and already tolerates sequence differences across the various targeted RAS protein variants, it is unlikely that resistance will emerge by spontaneous mutation, and we have not as yet observed tumor resistance in our in vivo studies with RRSP.

Thus, the combination of the highly effective RRSP with a robust easy to manufacture and implement delivery strategy could lead to pre-clinical and clinical development of a robust broadly applicable RAS degrader therapeutic.

MATERIALS AND METHODS

Chemicals, Protein purification, and Cell lines

All chemicals were from Sigma-Aldrich unless otherwise specified. An mRNA for expression of GFP (CleanCap *eGFP*-mRNA) and an mRNA for expression of the RAS/RAP1 protease (also known as *Vibrio vulnificus* MARTX toxin DUF5) (*rrsp*-mRNA) and a H451A catalytically inactive negative control mRNA (*rrsp**-mRNA) were synthesized by TriLink BioTechnologies. mRNA sequences were capped with 5' AG head (CleanCap®), hemagglutinin (HA)-tagged (as indicated) and polyadenylated tail and 100% pseudouridine (Table S2). Protein purification of RRSP-DT_B and RRSP*-DT_b for *in vivo* experiments were completed as described previously.[17] Cell lines were obtained from the National Cancer Institute RAS Initiative or collaborators. Cell lines were confirmed free of *Mycoplasma* using VenorGeM *Mycoplasma* Classic Endpoint PCR assay and were also subjected to short tandem repeat analysis using the AmpFLSTR Identifiler PCR Amplification Kit to authenticate the cell lines, comparing the results with information located at https://web.expasy.org/cellosaurus/. Cells were cultured at 37°C and 5% CO_2 atmosphere.

PANC-1 and KPC cells were grown in Dulbecco's Minimal Eagle's Medium (DMEM, American Type Culture Collection formulation) with 10% Fetal Bovine Serum (FBS) and 1% penicillin/streptomycin (P/S) and HCT-116 cells were grown in DMEM-F12 with Glutamax (Gibco) containing 10% FBS and 1% P/S.

Nanocarrier Formulation and characterization

To synthesize and load synthetic PEG-*b*-PPS nanocarriers with mRNA, block co-polymers PEG_{17}-*b*-PPS_{80}-pyridyl disulfide were synthesized and conjugated to the cationic dendritic peptide (DP) via disulfide exchange as previously described.[20] Briefly, good manufacturing practice (GMP) grade synthesis of PEG_{17}-*b*-PPS_{80}-pyridyl disulfide was performed in collaboration with the contract research organization Sequens Group, while the final DP-end capping was completed in-house within a clean room. The resulting sterile PPDP2 was mixed with *egfp*-mRNA, *rrsp*-mRNA or CleanCap® *mCherry*-mRNA (TriLink BioTechnologies) in 25 mM sodium acetate buffer at the weight ratio of 40:1 to assemble monodisperse spherical complexes for mRNA transfection or fluorescent tracing of cell transfection, respectively. For quality control, PPDP2-*egfp*-mRNA, PPDP2-*rrsp*-mRNA, and PPDP2-*mCherry*-mRNA nanocarriers were characterized using a Nano ZS Zetasizer (Malvern) and Azure 600 to ensure consistent nanocarrier diameter, concentration, structure, and nucleic acid loading efficiency, following previously established protocols.[20] Sample data of validation are shown in Figure S8.

Immunofluorescence

KPC and PANC-1 cells were plated on 4-well slides in DMEM (10% FBS, 1% P/S) media and allowed to attach overnight. The following day, 1 µg *egfp*-mRNA was mixed with 40 µg of PPDP2 in ddH_20 for 30 minutes at room temperature or 1.5 µL MessengerMax Lipofectamine (Invitrogen) as a positive control according to manufacturer's instructions. The mixture was added to cells along with negative controls, *egfp*-mRNA and nanocarriers alone. After 24-hour incubation, cells were washed three times for 5 minutes with phosphate-buffered saline (PBS), fixed with 100% methanol for 10 minutes, washed three times for 5 minutes with PBS, and mounted with 4′,6-diamidino-2-phenylindole (DAPI) stain. Cells were visualized on a Nikon Ti2 widefield microscope using a 40x objective. Five images were taken for each treatment and the total number of cells were counted per frame and compared to the number of cells that were expressing GFP.

SDS–PAGE and Western blotting

Protein extracts were prepared by either directly adding 2X sodium dodecyl sulfide (SDS)-polyacrylamide gel electrophoresis (PAGE) buffer to the tissue culture well or by harvesting cells by adding radioimmunoprecipitation assay (RIPA) buffer (50 mM Tris-HCl, pH 7.4, 150 mM NaCl, 2 mM EDTA, 1% Nonidet P-40, 1% Na-deoxycholate, 0.1% SDS), supplemented with cOmplete mini protease inhibitor cocktail (Roche, catalog. no 11836170001) and 1 mM phenylmethylsulfonyl fluoride (PMSF). Equal amounts of proteins or equal volumes were separated by SDS-PAGE followed by Western blot analysis as described previously (24). Membranes were blotted using the following antibodies: anti-panRAS (Thermo Fisher Scientific, catalog no. MA1-012, RRID:AB_2536664), which recognizes RAS Switch I and thus detects only uncleaved RAS. Anti–Phospho-p44/42 MAPK (pERK1/2; Cell Signaling Technology, catalog no. 4377, RRID:AB_331775), anti-p44/42 MAPK (ERK1/2; Cell Signaling Technology, catalog no. 4696, RRID:AB_390780), and anti-HB-EGF (Abcam, #ab185555). Anti-vinculin (Cell Signaling Technology, catalog no. 13901, RRID:AB_2728768) or anti-GAPDH (Cell Signaling Technology, catalog no. 2118S) (as indicated) was used for normalization. Secondary antibodies used were fluorescent-labeled IRDye 680RD goat anti-mouse (LI-COR Biosciences, catalog no. 926- 68070, RRID:AB_10956588) and IRDye 800CW goat anti-rabbit (LI-COR Biosciences, catalog no. 926-32211, RRID:AB_621843). Blot images were acquired using the Odyssey Infrared Imaging System (LI-COR Biosciences) and quantified by densitometry using NIH ImageJ software (ImageJ, RRID:SCR_003070). Percentage of uncleaved RAS and pERK/ERK was calculated as described previously.[18]

Protein extracts from frozen tissues were prepared by pulverizing tissue with mortar and pestle and homogenizing tissue in a microcentrifuge tube containing RIPA buffer. Samples were homogenized on ice three times, 5 seconds each time, incubated on ice for 30 minutes, and centrifuged at 22,400 x*g* for 15 minutes at 4 °C. Supernatants were collected and protein content measured using the BCA protein assay kit (Thermo Fisher Scientific) according to manufacturer's instructions.

Cytotoxicity and apoptosis assays

Apoptosis was assessed by Caspase-Glo 3/7 assay according to manufacturer's instructions (Promega). A total of 10,000 cells/well were grown in 24-well clear plates and treated with 5.5 µg (*in vivo* concentration) *rrsp*-mRNA or *rrsp**-mRNA by PPDP2 nanocarriers for 24 h. Caspase-Glo 3/7 was then added to each well and luminescence was recorded using a Tecan Safire2 plate reader.

Cytotoxicity was assessed by staining cells with crystal violet. Briefly, 2 x 10^4 cells/well were cultured in 24-well plates and treated with either 0.25, 0.5, 1, 1.5 or 2 µg *rrsp*-mRNA by PPDP2 nanocarriers or 2 µg *rrsp*-mRNA via MessengerMAX lipofectamine (Invitrogen) for 72 h. Cells were washed and crystal violet fixing/staining solution was added for 20 minutes at room temperature as described previously (20). Images of air-dried plates were acquired using a conventional desktop scanner.

For HCT-116 cells, cells were seeded into 12-well plate at ~1 x 10^5 cells per well overnight (~80% confluency). Cells were transfected with *egfp*-mRNA (8 µg) or *rrsp*-mRNA (8 µg, 4 µg, 1 µg, 0.5 µg) using MessengerMAX lipofectamine according to manufacturer's protocol. Images were taken using a ThermoScientific EVOS XL Core Imaging System AMEX1000 at indicted timepoints. Lysates were collected after 24 h and probed by Western blotting for total RAS as described previously.[16] For KPC cells, ~6.5 x 10^6 cells were seeded in a 12-well plate until cells were attached (~2 h). Once cells were attached, *rrsp*-mRNA was transfected into KPC cells using MessengerMAX lipofectamine. Cells were imaged over time using a Nikon Biostation CT. Calculation of percent confluency was done using Nikon Elements as described previously.[16]

***In vivo* tumors**

CBX tumors were initiated by subcutaneous injection of $2x10^6$ cultured PANC-1 PDAC cells to the dorsal flank of *nu/nu* mice. When tumors reached an average size of 80-120 mm^3, mice were randomized into four groups of five mice and intratumoral treatment was initiated. The first group received only PPDP2 synthetic nanocarriers (25 mM sodium acetate buffer), the second 0.25 mg/kg of PPDP2 + *rrsp*-mRNA (3X/week, excluding weekends), the third 0.25 mg/kg of PPDP2 + *rrsp**-mRNA (3X/week, excluding weekends), the fourth PPDP2 + *mCherry*-mRNA. Both tumor size and mouse body weight were measured every other day. At the end of the treatment schedule, mice were euthanized, tumors excised, and either snap frozen in liquid N_2 or fixed in 10% formalin overnight.

***In vivo* maximum tolerable dose in DTR mice**

In collaboration with Jackson Laboratory, we created a custom mouse model, expressing the DTR in all mouse cells by crossing the ROSA26iDTR mouse strain with the B6.FVB-Tg(EIIa-cre)C5379Lmgd/J strain to create DTR Knock-In mice. We divided the mice into seven treatment groups with five mice per treatment group and four mice in the control group. Treatments included 0.05 mg/kg RRSP-DT_B, 0.1 mg/kg RRSP-DT_B, 0.25 mg/kg RRSP-DT_B, 0.5 mg/kg of RRSP-DT_B, or 0.25 and 0.5 mg/kg of catalytically inactive RRSP*-DT_B delivere intraperitoneally. Mice were

treated, weighed, and assessed for signs of distress once per day, three times a week for four weeks. Median weights across all groups were recorded along with occurrence of deaths.

At the end of the experiment, tissue was harvested from heart, kidney, liver, lungs, and spleen from control group and highest dosed group to observe off-target effects. Peripheral blood mononuclear cells (PBMC) were harvested from blood via density gradient centrifugation over Ficoll and PBMCs were cultured for use in Western blotting of cell lysates with anti-HB-EGF (ThermoFisher Scientific, catalog no. IC259G) as per manufacturer's instructions and expression of HB-EGF was assessed by flow cytometry using the BD-FACSCelesta.

Histology, IHC, and image analysis

Paraffin-embedding, sectioning, hematoxylin and eosin (H&E) and immunohistochemistry (IHC) staining of mouse tissue specimens were performed by the Robert H. Lurie Comprehensive Cancer Center (RHLCCC) Mouse Histology and Pathology Core Facility. Tumor sections were stained with anti-cytokeratin 19 [(CK-19), #ab76539; Abcam], anti-Ki-67 (#GA626; Dako), anti-pan-RAS [(RAS), #PA5-85947; Thermo Fisher Scientific], anti-Phospho-p44/42 MAPK [(ERK1/2; Thr202/Tyr204, (D13.14.4E) XP, #4370; Cell Signaling Technology], anti-mCherry [Rockland Immunochemicals, catalog. no. 600-401-P16] antibodies as described previously (20). Primary antibodies were detected using the appropriate secondary antibodies and $3,3^0$-diaminobenzidine revelation (Dako).

Statistical analysis

Graphpad Prism v.8 software was used for statistical analysis. Bar plots represent the mean of at least three independent experiments and the standard deviation (SD) or standard error of the mean (SEM) as indicated in figure legends. Statistical significance was assessed using one-way ANOVA assuming normal distribution. Dunnett's multiple comparison post-test was employed to compare the mean of the control group with the mean of treatment groups. Tukey's multiple comparison test was used to compare the mean of each group with the mean of every other group. Values of $P < 0.05$ were considered statistically significant. Pairwise tests were analyzed using Student's *t*-test.

ACKNOWLEDGEMENTS

We would like to thank Wenan Qiang, Ph.D. and the Center for Developmental Therapeutics and Northwestern University for assistance with tumor engraftment. We would like to thank Young Rock Chung and Pablo Penaloza-MacMaster, Ph.D. for their assistance with validating the expression of DTR in our DTR Knock-In mice and Alfa Herrera for assistance with microscopy. This work was funded by Chicago Biomedical Consortium Accelerator Award (to K.J.F.S). This work was supported by the Northwestern University Interdepartmental ImmunoBiology Flow Cytometry Core Facility. Histology services were provided by the Northwestern University Research Histology and Phenotyping Laboratory which is supported by NCI P30-CA060553 awarded to the RHLCCC. Imaging work was performed at the Northwestern University Center for Advanced Microscopy generously supported by NCI CCSG P30 CA060553 awarded to the Robert H Lurie Comprehensive Cancer Center.

CONFLICTS OF INTEREST

T.E.E., Y.Q., E.A.S. and K.J.F.S. have filed a provisional patent through Northwestern University on PPDP2 delivery of *rrsp*-mRNA based on these studies. K.J.F.S. further discloses that she holds a patent on use of RRSP as a cancer therapeutic (Patent # US10829752B2) and is named on a patent on use of RRSP-DT_B to treat tumors (Patent #US 10597663B2). E.A.S. has a patent application for the PPDP2 delivery platform (US20240158814). E.A.S. is a founder of the company SNC Therapeutics which is developing PEG-*b*-PPS based therapeutics. K.J.F.S. has a significant interest in Situ Biosciences LLC, a contract research organization that conducts research unrelated to this work.

AUTHORS' CONTRIBUTIONS

T.E. Escher: Conceptualization, data curation, software, formal analysis, validation, investigation, visualization, methodology, writing–original draft, writing–review and editing. S.A. Yuk: Conceptualization, data curation, investigation, writing–review and editing. Y. Qian: Conceptualization, data curation, investigation, writing–review and editing. C.K. Stubbs: Conceptualization, data curation, formal analysis, investigation. E.A. Scott: Conceptualization, data curation, methodology, writing–review and editing. K.J. Satchell: Conceptualization, resources, data curation, supervision, funding acquisition, validation, investigation, methodology, writing–original draft, project administration, writing–review and editing.

REFERENCES

1. Siegel, R.L., Miller, K.D., Wagle, N.S., and Jemal, A. (2023). Cancer statistics, 2023. CA: A Cancer Journal for Clinicians *73*, 17-48. https://doi.org/10.3322/caac.21763.
2. Pezzilli, R., Fabbri, D., and Imbrogno, A. (2012). Pancreatic ductal adenocarcinoma screening: new perspectives. World J Gastroenterol *18*, 4973-4977. 10.3748/wjg.v18.i36.4973.
3. Hezel, A.F., Kimmelman, A.C., Stanger, B.Z., Bardeesy, N., and Depinho, R.A. (2006). Genetics and biology of pancreatic ductal adenocarcinoma. Genes Dev *20*, 1218-1249. 10.1101/gad.1415606.
4. McCormick, F. (2019). Progress in targeting RAS with small molecule drugs. Biochem J *476*, 365-374. 10.1042/BCJ20170441.
5. McGee, J.H., Shim, S.Y., Lee, S.J., Swanson, P.K., Jiang, S.Y., Durney, M.A., and Verdine, G.L. (2018). Exceptionally high-affinity Ras binders that remodel its effector domain. J Biol Chem *293*, 3265-3280. 10.1074/jbc.M117.816348.
6. Martin-Acosta, P., and Xiao, X. (2021). PROTACs to address the challenges facing small molecule inhibitors. Eur J Med Chem *210*, 112993. 10.1016/j.ejmech.2020.112993.
7. Xi, M., Chen, Y., Yang, H., Xu, H., Du, K., Wu, C., Xu, Y., Deng, L., Luo, X., Yu, L., Wu, Y., et al. (2019). Small molecule PROTACs in targeted therapy: An emerging strategy to induce protein degradation. Eur J Med Chem *174*, 159-180. 10.1016/j.ejmech.2019.04.036.
8. Yao, T., Xiao, H., Wang, H., and Xu, X. (2022). Recent Advances in PROTACs for Drug Targeted Protein Research. Int J Mol Sci *23*. 10.3390/ijms231810328.
9. Bobbala, S., Allen, S.D., Yi, S., Vincent, M., Frey, M., Karabin, N.B., and Scott, E.A. (2020). Employing bicontinuous-to-micellar transitions in nanostructure morphology for on-demand photo-oxidation responsive cytosolic delivery and off–on cytotoxicity. Nanoscale *12*, 5332-5340. 10.1039/C9NR10921H.
10. Burke, J.A., Zhang, X., Bobbala, S., Frey, M.A., Bohorquez Fuentes, C., Freire Haddad, H., Allen, S.D., Richardson, R.A.K., Ameer, G.A., and Scott, E.A. (2022). Subcutaneous nanotherapy repurposes the immunosuppressive mechanism of rapamycin to enhance allogeneic islet graft viability. Nat Nanotechnol *17*, 319-330. 10.1038/s41565-021-01048-2.
11. Dowling, D.J., Scott, E.A., Scheid, A., Bergelson, I., Joshi, S., Pietrasanta, C., Brightman, S., Sanchez-Schmitz, G., Van Haren, S.D., Ninkovic, J., Kats, D., et al. (2017). Toll-like receptor 8 agonist nanoparticles mimic immunomodulating effects of the live BCG vaccine

and enhance neonatal innate and adaptive immune responses. J Allergy Clin Immunol *140*, 1339-1350. 10.1016/j.jaci.2016.12.985.

12. Escher, T.E., and Satchell, K.J.F. (2023). RAS Degraders: The New Frontier for RAS Driven Cancers. Molecular Therapy. https://doi.org/10.1016/j.ymthe.2023.03.017.
13. Antic, I., Biancucci, M., and Satchell, K.J. (2014). Cytotoxicity of the Vibrio vulnificus MARTX toxin effector DUF5 is linked to the C2A subdomain. Proteins *82*, 2643-2656. 10.1002/prot.24628.
14. Antic, I., Biancucci, M., Zhu, Y., Gius, D.R., and Satchell, K.J.F. (2015). Site-specific processing of Ras and Rap1 Switch I by a MARTX toxin effector domain. Nat Commun *6*, 7396. 10.1038/ncomms8396.
15. Biancucci, M., Rabideau, A.E., Lu, Z., Loftis, A.R., Pentelute, B.L., and Satchell, K.J.F. (2017). Substrate Recognition of MARTX Ras/Rap1-Specific Endopeptidase. Biochemistry *56*, 2747-2757. 10.1021/acs.biochem.7b00246.
16. Stubbs, C.K., Biancucci, M., Vidimar, V., and Satchell, K.J.F. (2021). RAS specific protease induces irreversible growth arrest via p27 in several KRAS mutant colorectal cancer cell lines. Sci Rep *11*, 17925. 10.1038/s41598-021-97422-0.
17. Vidimar, V., Park, M., Stubbs, C.K., Ingram, N.K., Qiang, W., Zhang, S., Gursel, D., Melnyk, R.A., and Satchell, K.J.F. (2022). Proteolytic pan-RAS Cleavage Leads to Tumor Regression in Patient-derived Pancreatic Cancer Xenografts. Mol Cancer Ther *21*, 810-820. 10.1158/1535-7163.MCT-21-0550.
18. Vidimar, V., Beilhartz, G.L., Park, M., Biancucci, M., Kieffer, M.B., Gius, D.R., Melnyk, R.A., and Satchell, K.J.F. (2020). An engineered chimeric toxin that cleaves activated mutant and wild-type RAS inhibits tumor growth. Proc Natl Acad Sci U S A *117*, 16938-16948. 10.1073/pnas.2000312117.
19. Yi, S., Allen, S.D., Liu, Y.G., Ouyang, B.Z., Li, X., Augsornworawat, P., Thorp, E.B., and Scott, E.A. (2016). Tailoring Nanostructure Morphology for Enhanced Targeting of Dendritic Cells in Atherosclerosis. ACS Nano *10*, 11290-11303. 10.1021/acsnano.6b06451.
20. Yi, S., Kim, S.Y., Vincent, M.P., Yuk, S.A., Bobbala, S., Du, F., and Scott, E.A. (2022). Dendritic peptide-conjugated polymeric nanovectors for non-toxic delivery of plasmid DNA and enhanced non-viral transfection of immune cells. iScience *25*, 104555. 10.1016/j.isci.2022.104555.
21. Cai, W., Luo, T., Chen, X., Mao, L., and Wang, M. A Combinatorial Library of Biodegradable Lipid Nanoparticles Preferentially Deliver mRNA into Tumor Cells to Block

Mutant RAS Signaling. Advanced Functional Materials *n/a*, 2204947. https://doi.org/10.1002/adfm.202204947.

22. Allen, S.D., Bobbala, S., Karabin, N.B., Modak, M., and Scott, E.A. (2018). Benchmarking Bicontinuous Nanospheres against Polymersomes for in Vivo Biodistribution and Dual Intracellular Delivery of Lipophilic and Water-Soluble Payloads. ACS Appl Mater Interfaces *10*, 33857-33866. 10.1021/acsami.8b09906.
23. Allen, S.D., Liu, Y.-G., Bobbala, S., Cai, L., Hecker, P.I., Temel, R., and Scott, E.A. (2018). Polymersomes scalably fabricated via flash nanoprecipitation are non-toxic in non-human primates and associate with leukocytes in the spleen and kidney following intravenous administration. Nano Research *11*, 5689-5703. 10.1007/s12274-018-2069-x.
24. Vincent, M.P., Navidzadeh, J.O., Bobbala, S., and Scott, E.A. (2022). Leveraging self-assembled nanobiomaterials for improved cancer immunotherapy. Cancer Cell *40*, 255-276. 10.1016/j.ccell.2022.01.006.
25. Morgun, E., Zhu, J., Almunif, S., Bobbala, S., Aguilar, M.S., Wang, J., Conner, K., Cui, Y., Cao, L., Seshadri, C., Scott, E.A., et al. (2023). Vaccination with mycobacterial lipid loaded nanoparticle leads to lipid antigen persistence and memory differentiation of antigen-specific T cells. Elife *12*. 10.7554/eLife.87431.
26. Vincent, M.P., Karabin, N.B., Allen, S.D., Bobbala, S., Frey, M.A., Yi, S., Yang, Y., and Scott, E.A. (2021). The Combination of Morphology and Surface Chemistry Defines the Immunological Identity of Nanocarriers in Human Blood. Adv Ther (Weinh) *4*. 10.1002/adtp.202100062.
27. Gill, D.M. (1982). Bacterial toxins: a table of lethal amounts. Microbiol Rev *46*, 86-94. 10.1128/mr.46.1.86-94.1982.
28. Ebi, Y.A.a.H. (2023). Inhibition of the MAPK pathway induces re-localization of membranous proteins, leading to adaptive resistance to KRAS G12C inhibitor mediated by YAP-induced MRAS. RAS Dialogue Blog
29. Bernard, V., Fleming, J., and Maitra, A. (2016). Molecular and Genetic Basis of Pancreatic Carcinogenesis: Which Concepts May be Clinically Relevant? Surg Oncol Clin N Am *25*, 227-238. 10.1016/j.soc.2015.11.003.
30. A Phase 1/2, Study Evaluating the Safety, Tolerability, PK, and Efficacy of Sotorasib (AMG 510) in Subjects With Solid Tumors With a Specific KRAS Mutation (CodeBreaK 100).
31. Biancucci, M., Minasov, G., Banerjee, A., Herrera, A., Woida, P.J., Kieffer, M.B., Bindu, L., Abreu-Blanco, M., Anderson, W.F., Gaponenko, V., Stephen, A.G., et al. (2018). The

bacterial Ras/Rap1 site-specific endopeptidase RRSP cleaves Ras through an atypical mechanism to disrupt Ras-ERK signaling. Sci Signal *11*. 10.1126/scisignal.aat8335.

32. Janne, P.A. (2023). Progress in the treatment of KRAS mutant cancers. .

33. Bobbala, S., Allen, S.D., Yi, S., Vincent, M., Frey, M., Karabin, N.B., and Scott, E.A. (2020). Employing bicontinuous-to-micellar transitions in nanostructure morphology for on-demand photo-oxidation responsive cytosolic delivery and off-on cytotoxicity. Nanoscale *12*, 5332-5340. 10.1039/c9nr10921h.

34. Yi, S., Zhang, X., Sangji, M.H., Liu, Y., Allen, S.D., Xiao, B., Bobbala, S., Braverman, C.L., Cai, L., Hecker, P.I., DeBerge, M., et al. (2019). Surface Engineered Polymersomes for Enhanced Modulation of Dendritic Cells During Cardiovascular Immunotherapy. Advanced Functional Materials *29*, 1904399. 10.1002/adfm.201904399.

35. Allen, S., Osorio, O., Liu, Y.G., and Scott, E. (2017). Facile assembly and loading of theranostic polymersomes via multi-impingement flash nanoprecipitation. J Control Release *262*, 91-103. 10.1016/j.jconrel.2017.07.026.

36. Allen, S., Vincent, M., and Scott, E. (2018). Rapid, Scalable Assembly and Loading of Bioactive Proteins and Immunostimulants into Diverse Synthetic Nanocarriers Via Flash Nanoprecipitation. J Vis Exp. 10.3791/57793.

37. Awad, M.M., Liu, S., Rybkin, II, Arbour, K.C., Dilly, J., Zhu, V.W., Johnson, M.L., Heist, R.S., Patil, T., Riely, G.J., Jacobson, J.O., et al. (2021). Acquired Resistance to KRAS(G12C) Inhibition in Cancer. N Engl J Med *384*, 2382-2393. 10.1056/NEJMoa2105281.

38. Zhao, Y., Murciano-Goroff, Y.R., Xue, J.Y., Ang, A., Lucas, J., Mai, T.T., Da Cruz Paula, A.F., Saiki, A.Y., Mohn, D., Achanta, P., Sisk, A.E., et al. (2021). Diverse alterations associated with resistance to KRAS(G12C) inhibition. Nature *599*, 679-683. 10.1038/s41586-021-04065-2.

39. Tanaka, N., Lin, J.J., Li, C., Ryan, M.B., Zhang, J., Kiedrowski, L.A., Michel, A.G., Syed, M.U., Fella, K.A., Sakhi, M., Baiev, I., et al. (2021). Clinical Acquired Resistance to KRAS(G12C) Inhibition through a Novel KRAS Switch-II Pocket Mutation and Polyclonal Alterations Converging on RAS-MAPK Reactivation. Cancer Discov *11*, 1913-1922. 10.1158/2159-8290.CD-21-0365.

40. Suzuki, S., Yonesaka, K., Teramura, T., Takehara, T., Kato, R., Sakai, H., Haratani, K., Tanizaki, J., Kawakami, H., Hayashi, H., Sakai, K., et al. (2021). KRAS Inhibitor Resistance in MET-Amplified KRAS (G12C) Non-Small Cell Lung Cancer Induced By

RAS- and Non-RAS-Mediated Cell Signaling Mechanisms. Clin Cancer Res *27*, 5697-5707. 10.1158/1078-0432.CCR-21-0856.

41. Adachi, Y., Kimura, R., Hirade, K., Yanase, S., Nishioka, Y., Kasuga, N., Yamaguchi, R., and Ebi, H. (2023). Scribble mis-localization induces adaptive resistance to KRAS G12C inhibitors through feedback activation of MAPK signaling mediated by YAP-induced MRAS. Nat Cancer *4*, 829-843. 10.1038/s43018-023-00575-2.

SUPPLEMENTAL INFORMATION

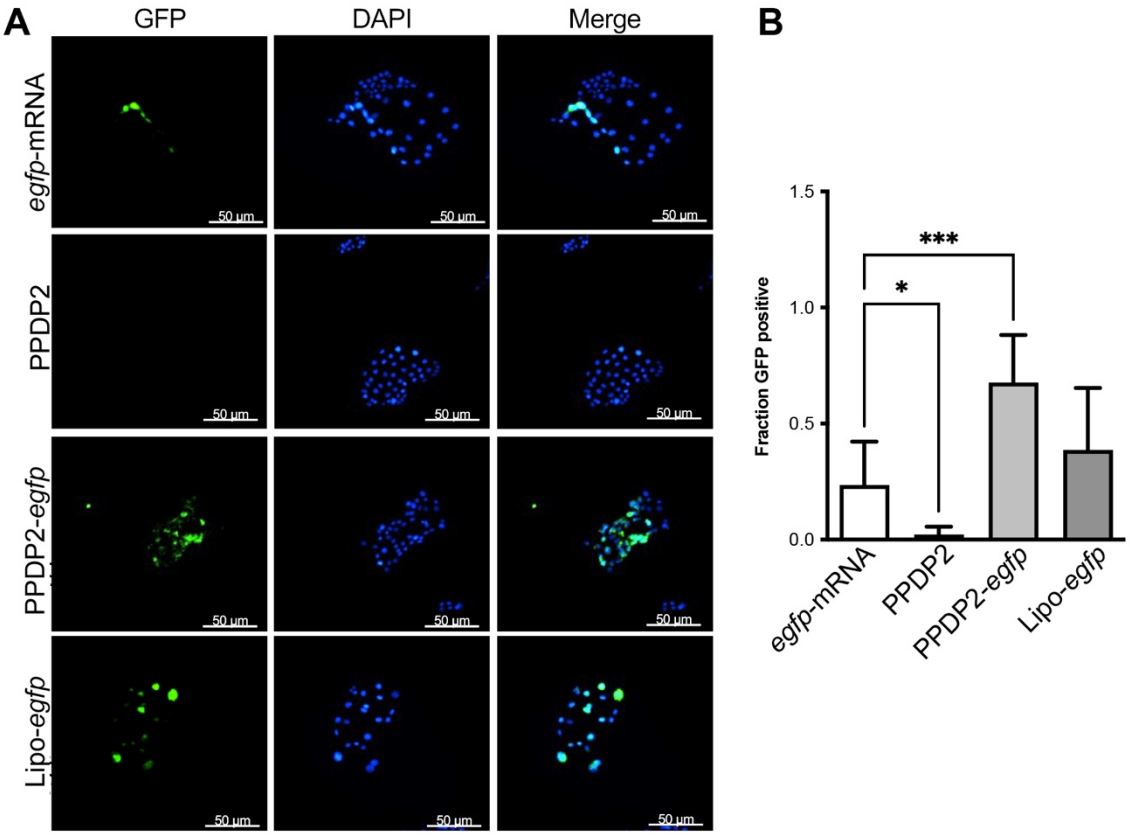

Figure S1. PPDP2 delivery of *egfp*-mRNA to KPC cells

(A) Representative fluorescent images of KPC cells after transfection of cells with 1 µg of *egfp*-mRNA alone, PPDP2 alone (1:40 w/v%), *egfp*-mRNA with PPDP2 (PPDP2-*egfp*) or *egfp*-mRNA with Lipofectamine MessengerMAX (Lipo-*egfp*). **(B)** Quantification of the fraction of GFP positive cells (green) from five imaged frames are shown as a histogram (n=5). P values were calculated using a one-way ANOVA and Dunnett's multiple comparisons test, *p<0.05, ***p<0.001.

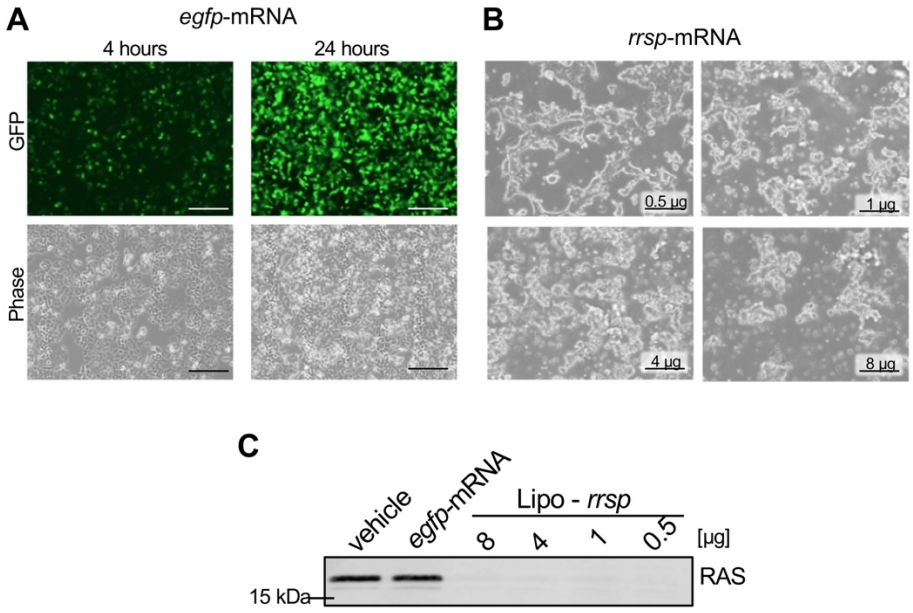

Figure S2. HCT-116 cells transfected with *rrsp*-mRNA inhibits proliferation and reduces RAS expression. (A) GFP fluorescence and phase images of HCT-116 cells following mRNA transfection with capped *egfp*-mRNA using MessengerMAX lipofectamine for time indicated **(B)** Representative images of HCT-116 cells transfected with *rrsp*-mRNA transfected after 24 h using µg of mRNA indicated. **(C)** Western blot using anti-pan-RAS antibody of cell lysates prepared from images in B. Pan-RAS antibody detects the cleaved Switch 1 so no band indicates 100% degradation.

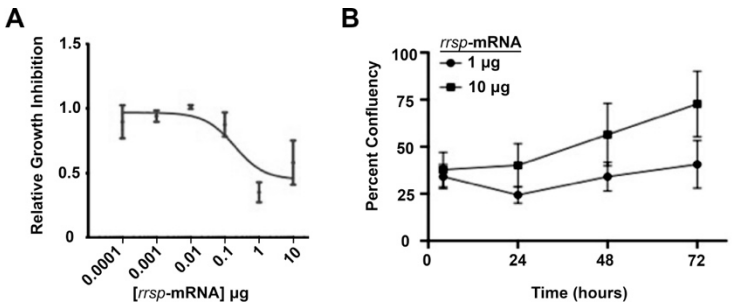

Figure S3. Transfection with *rrsp*-mRNA causes cell death in mouse pancreatic KPC cells. **(A)** Dose response to KPC cells transfected with six different doses of *rrsp*-mRNA with MessengerMAX mRNA. **(B)** Relative growth after treatment with 1 or 10 µg of rrsp mRNA. (compared to PBS control) from time-lapse images taken 24-, 48-, or 72-h following transfection.

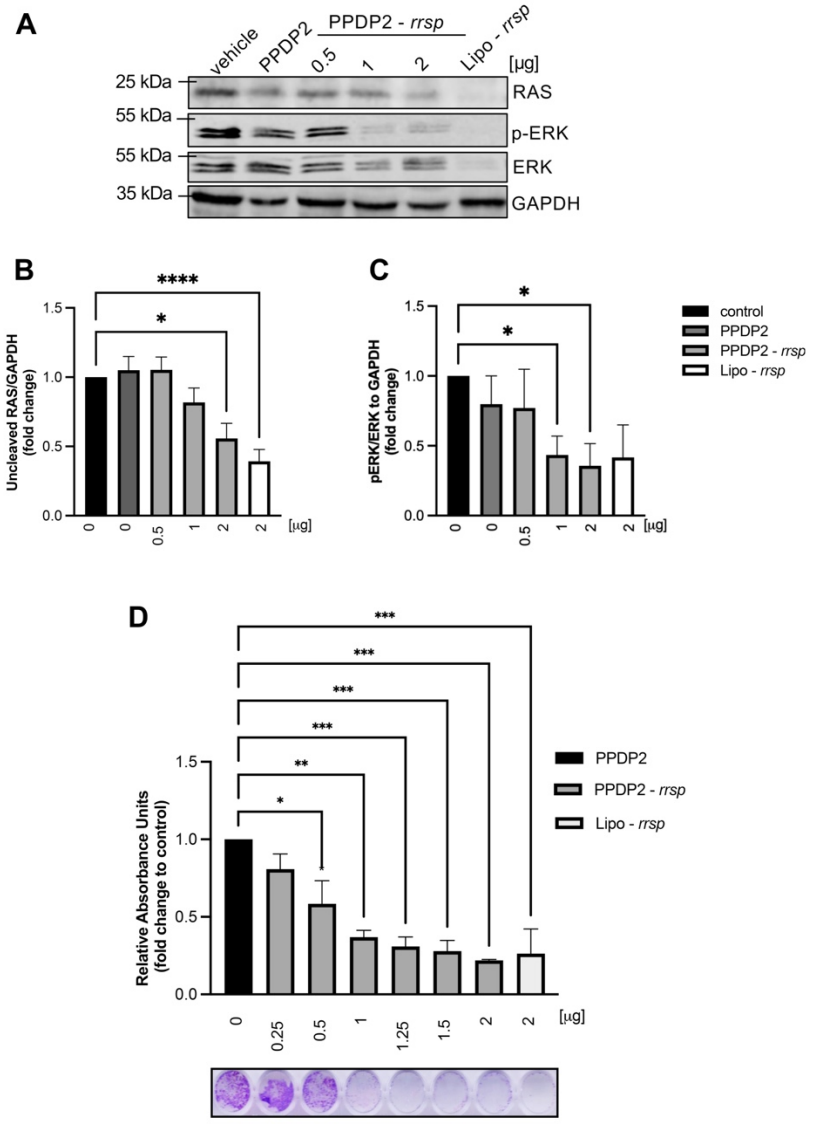

771

772 **Figure S4. PPDP2-*rrsp* reduces levels of RAS and impacts cell proliferation in KPC cells.**
773 **(A-C)** Representative Western blot (A) and densitometry quantification (*n=5)* of
774 uncleaved/cleaved RAS (B) and pERK (C) levels of KPC cells transfected for 24 h with either
775 vehicle only, PPDP2, PPDP2 nanocarriers loaded with *rrsp*-mRNA (PPDP2-*rrsp*) or *rrsp* mixed
776 with MessengerMAX lipofectamine (Lipo-*rrsp*) as indicated. **(D)** Spectrophotometric quantification
777 *(n=3)* and representative images of crystal violet-stained colonies from KPC cells treated as
778 indicated. Data are presented as mean ± SEM with $n \geq 5$. *P* values were calculated using a one-
779 way ANOVA and Dunnett's multiple comparisons test, * $p < 0.05$, ** $p < 0.01$, *** $p < 0.001$.

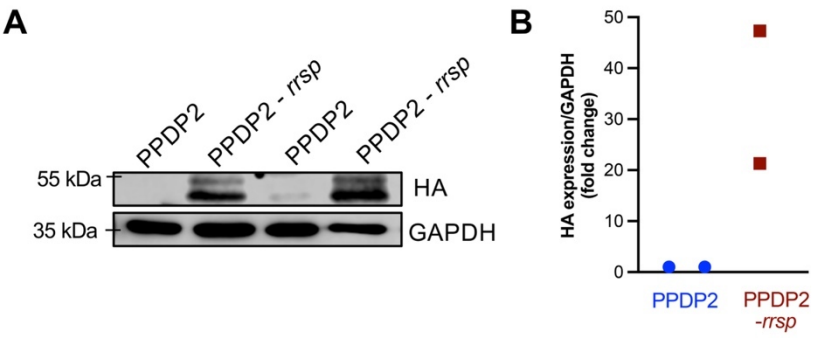

780

781

782 **Figure S5. Protein expression in frozen resected tumors. Lysates were prepared from**
783 **resected tumors. (A)** Expression of HA-tagged RRSP from *rrsp*-mRNA in representative
784 PPDP2 only and PPDP2-rrsp-mRNA treated tumors. **(B)** Quantification expressed as fold
785 change for blot in Panel A.

786

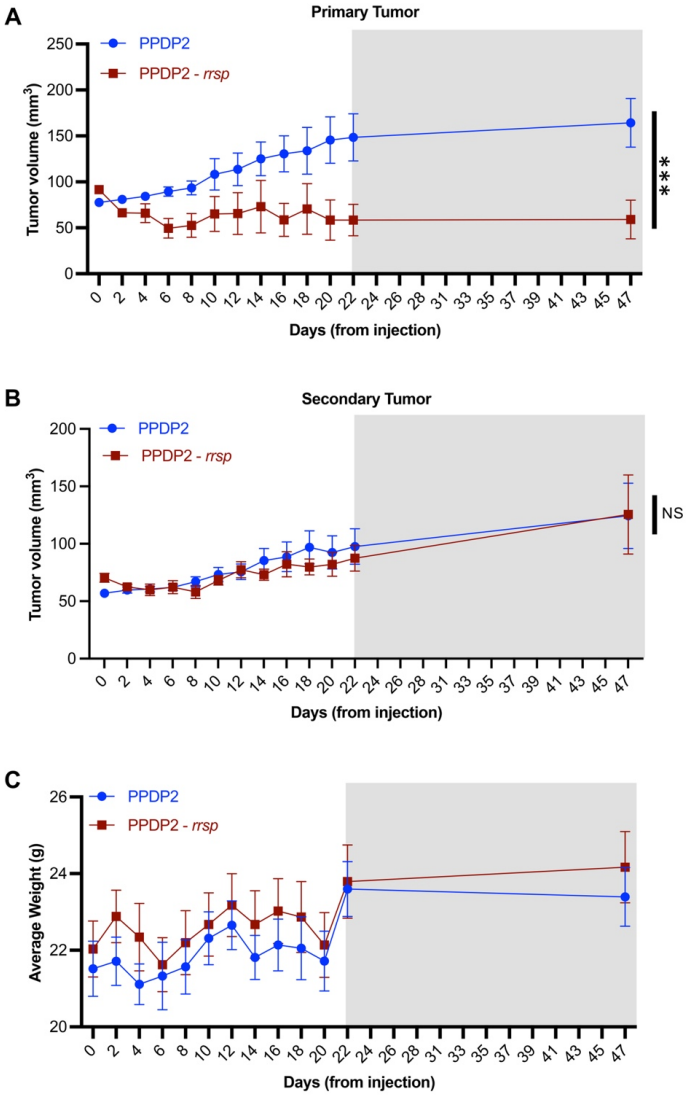

787

788 **Figure S6. PPDP2-*rrsp*-mRNA does not disseminate to reduce a secondary tumor. (A,B)**
789 PANC-1 xenograft tumors were established on both flanks of a single *nu/nu* mouse. Tumor
790 volume was measured every other day, excluding weekends for the both primary tumor that was
791 treated (A) and the opposite flank that received no treatment (B). Day 0 indicates day of first
792 treatment with 0.25 mg/kg dose of PPDP2-*rrsp*-mRNA (red) three times per week compared to
793 PPDP2 alone (blue). Grey shaded area indicates time of no treatment to test for tumor regrowth
794 **(C)** Weight of mice measured every other day. Data were presented as mean ± SEM with $n = 5$.
795 P values were calculated using a one-way ANOVA and Dunnett's multiple comparisons test,
796 NS=not significant, *** $p < 0.001$.

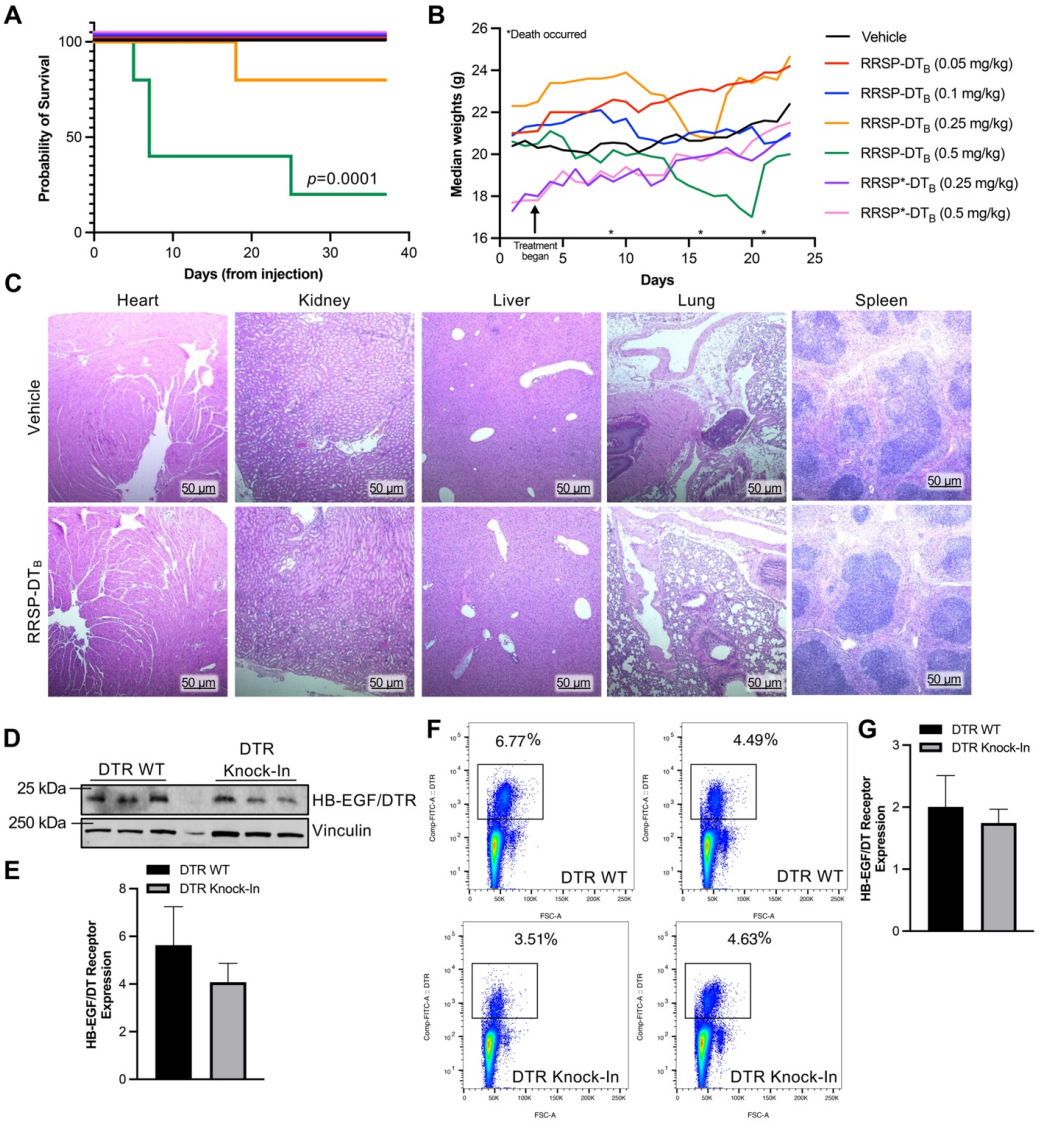

Figure S7. Maximum tolerated dose and off-target effects of RRSP protein delivery to all cells. (A) Survival curve from mice treated with vehicle, RRSP-DT_B or RRSP*-DT_B treated DTR mice at indicated dose. **(B)** Median weights across all groups are reported along with occurrence of deaths. **(C)** H&E-stained tissue from heart, kidney, liver, lungs, and spleen from vehicle and 0.5 mg/kg RRSP-DT_B. **(D)** Western blot assay and **(E)** quantification (*n*=3) of HB-EGF/DTR receptor expression from PBMCs collected from control DTR WT mice and DTR Knock-In mice. **(F)** Flow cytometry analysis against DTR antibody on duplicate samples from mouse PBMCs. **(G)** Quantification of flow cytometry (*n*=3)

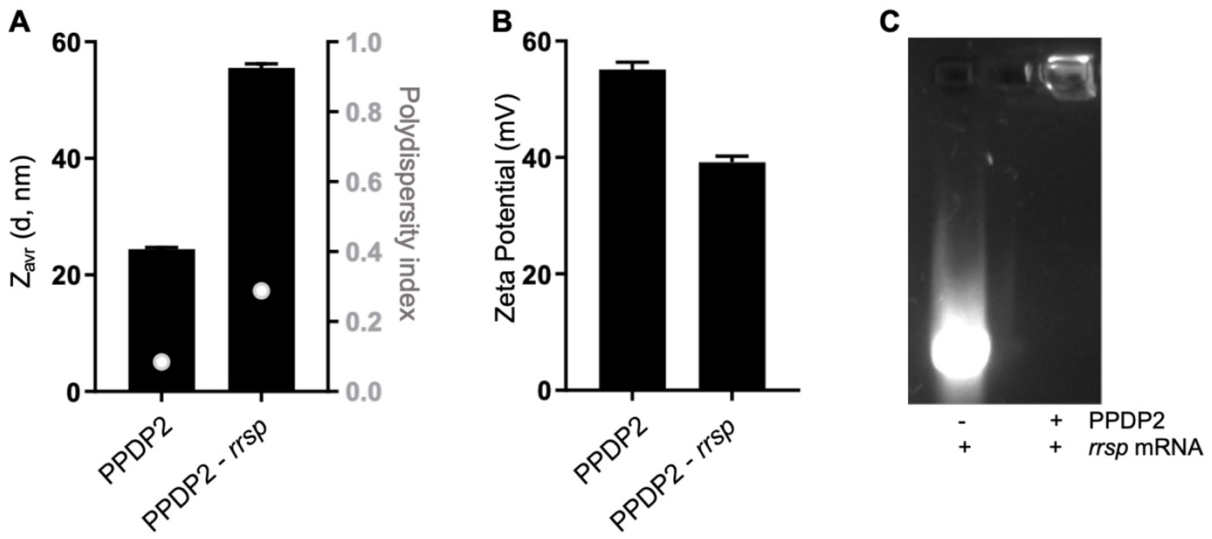

Figure S8. Sample data on PPDP2 loading of *rrsp*-mRNA. (A) *Z*-average size of PPDP2 alone and PPDP2 loaded with *rrsp*-mRNA. Polydispersity index (*y*-2 axis, grey) of PPDP2 alone and PPDP2 loaded with *rrsp*-mRNA shown as white/grey marker. **(C)** Zeta potential of PPDP2 alone and PPDP2 loaded with *rrsp*-mRNA. (D) Gel electrophoresis of naked rrsp-mRNA and PPDP2/*rrsp*-mRNA nanocomplexes at a 40:1 wt. ratio, demonstrating retention and immobility of mRNA within wells following stable complexation with PPDP2.

818 Table S1. Structure based prediction of residues of RRSP that contact KRAS

KRAS residue		RRSP residue		Domain	Distance (Å)	Interaction
Met	1	Pro	225	C2A	3.99	hydrophobic
Met	1	Ile	226	C2A	3.41	hydrophobic
Lys	5	Glu	218	C2A	2.66	salt bridge hydrogen bond
Ile	24	Asn	401	C2B	3.60	induction + dispersion
Ile	24	Gln	403	C2B	3.89	induction + dispersion
Gln	25	Arg	399	C2B	3.78	electrostatic
Gln	25	Asn	401	C2B	3.18	electrostatic
Gln	25	Gly	404	C2B	3.28	induction + dispersion
His	27	Arg	399	C2B	3.07	ionic repulsion CAUTION
His	27	Glu	406	C2B	3.91	salt bridge hydrogen bond anion-π stacking
His	27	Leu	409	C2B	3.08	induction + dispersion
Val	29	Arg	399	C2B	3.07	induction + dispersion
Glu	31	Leu	409	C2B	3.76	induction + dispersion
Glu	31	Ala	440	C2B	3.03	induction + dispersion
Glu	31	His	445	C2B	3.37	salt bridge hydrogen bond anion-π stacking
Tyr	32	His	313	C2B	2.99	cation-π stacking π-π stacking hydrogen bond dipole-π stacking
Tyr	32	His	342	C2B	3.72	cation-π stacking π-π stacking hydrogen bond dipole-π stacking
Tyr	32	Lys	372	C2B	3.46	cation-π stacking hydrogen bond
Asp	33	Arg	399	C2B	3.35	salt bridge hydrogen bond
Pro	34	Gln	201	C2A	3.84	induction + dispersion
Pro	34	Arg	344	C2B	3.43	induction + dispersion
Pro	34	Lys	372	C2B	2.81	induction + dispersion
Pro	34	Asp	393	C2B	3.21	induction + dispersion
Pro	34	Arg	412	C2B	3.31	induction + dispersion
Thr	35	Gln	198	C2A	3.77	electrostatic
Thr	35	Gln	201	C2A	3.59	electrostatic
Thr	35	Arg	344	C2B	2.89	electrostatic
Thr	35	Ala	398	C2B	3.81	induction + dispersion
Ile	36	Gln	201	C2A	2.64	induction + dispersion
Glu	37	Tyr	197	C2A	2.65	anion-π stacking π-π stacking electrostatic
Glu	37	Gln	201	C2A	3.48	electrostatic
Glu	37	Ser	230	C2A	3.18	electrostatic
Glu	37	Ala	231	C2A	3.71	induction + dispersion
Glu	37	Glu	232	C2A	3.88	ionic repulsion CAUTION
Asp	38	Lys	217	C2A	2.57	salt bridge hydrogen bond
Ser	39	Lys	217	C2A	3.57	electrostatic
Arg	41	Lys	221	C2A	3.76	ionic repulsion CAUTION

Arg	41	Asp	224	C2A	2.91	salt bridge hydrogen bond
Arg	41	Ser	227	C2A	3.00	electrostatic
Arg	41	Gly	228	C2A	3.26	induction + dispersion
Arg	41	Asp	229	C2A	2.74	salt bridge hydrogen bond
Arg	41	Ile	234	C2A	2.94	induction + dispersion
Leu	52	Pro	225	C2A	3.44	hydrophobic
Leu	52	Ser	227	C2A	3.67	induction + dispersion
Leu	52	Gly	228	C2A	3.93	hydrophobic
Asp	54	Lys	221	C2A	2.74	salt bridge hydrogen bond
Gln	61	Gln	210	C2A	2.74	electrostatic
Glu	63	Lys	370	C2B	2.67	salt bridge hydrogen bond
Tyr	64	Thr	204	C2A	3.73	electrostatic
Tyr	64	Gly	205	C2A	2.78	hydrophobic
Tyr	64	Glu	207	C2A	3.06	anion-π stacking π-π stacking electrostatic
Tyr	64	Gln	210	C2A	2.90	electrostatic
Tyr	64	Lys	370	C2B	2.83	cation-π stacking hydrogen bond
Ser	65	Glu	207	C2A	2.95	electrostatic
Ala	66	Trp	169	C2A	4.00	hydrophobic
Ala	66	Glu	207	C2A	2.75	induction + dispersion
Ala	66	Met	211	C2A	3.83	hydrophobic
Met	67	Glu	207	C2A	3.59	electrostatic
Met	67	Gln	210	C2A	3.31	electrostatic
Met	67	Met	211	C2A	3.41	hydrophobic electrostatic
Met	67	Tyr	214	C2A	3.27	electrostatic
Gln	70	Met	211	C2A	3.97	electrostatic
Gln	70	Tyr	214	C2A	3.48	electrostatic
Tyr	71	Tyr	214	C2A	3.51	hydrogen bond π-π stacking dipole-π stacking hydrophobic
Thr	74	Tyr	214	C2A	3.04	electrostatic

819

820

821 Table S2. Sequences of mRNA molecules commercially synthesized for this study.

	mRNA sequences (5'-3')
egfp-mRNA	AUGGUGAGCAAGGGCGAGGAGCUGUUCACCGGGGUGGUGCCCAUCCUGGUCGAGCUGGAC GGCGACGUAAACGGCCACAAGUUCAGCGUGUCCGGCGAGGGCGAGGGCGAUGCCACCUACG GCAAGCUGACCCUGAAGUUCAUCUGCACCACCGGCAAGCUGCCCGUGCCCUGGCCCACCCU CGUGACCACCCUGACCUACGGCGUGCAGUGCUUCAGCCGCUACCCCGACCACAUGAAGCAG CACGACUUCUUCAAGUCCGCCAUGCCCGAAGGCUACGUCCAGGAGCGCACCAUCUUCUUCAA GGACGACGGCAACUACAAGACCCGCGCCGAGGUGAAGUUCGAGGGCGACACCCUGGUGAAC CGCAUCGAGCUGAAGGGCAUCGACUUCAAGGAGGACGGCAACAUCCUGGGGCACAAGCUGG AGUACAACUACAACAGCCACAACGUCUAUAUCAUGGCCGACAAGCAGAAGAACGGCAUCAAG GUGAACUUCAAGAUCCGCCACAACAUCGAGGACGGCAGCGUGCAGCUCGCCGACCACUACCA GCAGAACACCCCCAUCGGCGACGGCCCCGUGCUGCUGCCCGACAACCACUACCUGAGCACC CAGUCCGCCCUGAGCAAAGACCCCAACGAGAAGCGCGAUCACAUGGUCCUGCUGGAGUUCG UGACCGCCGCCGGGAUCACUCUCGGCAUGGACGAGCUGUACAAGUAA
rrsp-*mRNA* – HA Tag	ATGGGTGATAAAACCAAGGTCGTGGTCGATTTAGCGCAAATCTTTACGGTGCAAGAGCTGAAAG AAAGAGCAAAAGTTTTTGCTAAACCGATTGGCGCATCCTACCAAGGTATTCTCGATCAACTCGAC CTTGTGCATCAGGCTAAAGGCCGCGATCAAATCGCAGCGAGCTTTGAGCTTAATAAGAAGATTA ATGACTACATCGCTGAACATCCAACTTCGGGGCGTAATCAAGCGCTAACGCAGTTGAAAGAGCA GGTCACCAGTGCGTTGTTTATCGGTAAGATGCAAGTTGCCCAAGCGGGTATTGATGCAATCGCA CAAACAAGACCGGAGCTTGCCGCTCGTATCTTTATGGTCGCGATTGAAGAAGCCAACGGTAAAC ACGTAGGTTTGACGGACATGATGGTTCGTTGGGCCAATGAAGACCCATACTTGGCACCGAAGC ATGGTTACAAAGGCGAAACGCCAAGTGACCTTGGTTTTGATGCGAAGTACCACGTAGATCTAGG TGAGCATTACGCTGATTTCAAACAGTGGTTAGAAACGTCCCAGTCGAACGGGTTGTTGAGTAAA GCGACGTTGGATGAATCCACTAAAACGGTTCATCTTGGCTATAGCTATCAAGAACTTCAGGATTT GACGGGTGCTGAATCGGTGCAAATGGCGTTCTACTTCCTGAAAGAAGCGGCGAAGAAAGCGGA TCCGATTTCTGGTGATTCAGCTGAAATGATACTGCTGAAGAAATTTGCAGATCAAAGCTACTTAT CTCAACTTGATTCCGACCGAATGGATCAAATTGAAGGTATCTACCGCAGTAGCCATGAGACGGA TATTGACGCTTGGGATCGTCGTTACTCTGGTACAGGCTATGATGAGCTGACGAATAAGCTTGCT AGTGCAACGGGCGTTGACGAGCAGCTTGCGGTTCTTCTGGATGATCGTAAAGGCCTCTTGATTG GTGAAGTGCATGGCAGCGACGTCAACGGCCTACGCTTTGTTAATGAACAGATGGATGCACTGAA AAAACAGGGAGTCACAGTCATTGGCCTTGAGCATTTACGCTCAGACCTTGCGCAACCGCTGATT GATCGCTACCTAGCTACGGGTGTGATGTCGAGTGAACTAAGCGCAATGCTGAAAACAAAGCATC TCGATGTCACTCTTTTTGAAAACGCACGTGCTAACGGTATGCGCATCGTCGCGCTGGATGCAAA CAGCTCTGCGCGTCCAAATGTTCAGGGAACAGAACATGGTCTGATGTACCGTGCTGGTGCTGC GAACAACATTGCGGTGGAAGTATTACAAAATCTGCCTGATGGCGAAAAGTTCGTTGCTATCTAC GGTAAAGCGCATTTGCAGTCTCACAAAGGGATTGAAGGGTTCGTTCCTGGTATCACGCACCGTC TCGATCTTCCTGCGCTTAAAGTCAGTGACTCGAACCAGTTCACAGTTGAACAAGACGATGTAAG TCTACGTGTTGTCTACGATGATGTTGCTAACAAACCGAAGATCACGTTCAAGGGCAGTTTGTAG
*rrsp** mRNA – HA Tag	ATGTACCCATACGTTCCAGATTACGCTATGGGTGATAAAACCAAGGTCGTGGTCGATTTAGCGC AAATCTTTACGGTGCAAGAGCTGAAAGAAAGAGCAAAAGTTTTTGCTAAACCGATTGGCGCATC CTACCAAGGTATTCTCGATCAACTCGACCTTGTGCATCAGGCTAAAGGCCGCGATCAAATCGCA

	GCGAGCTTTGAGCTTAATAAGAAGATTAATGACTACATCGCTGAACATCCAACTTCGGGGCGTA ATCAAGCGCTAACGCAGTTGAAAGAGCAGGTCACCAGTGCGTTGTTTATCGGTAAGATGCAAGT TGCCCAAGCGGGTATTGATGCAATCGCACAAACAAGACCGGAGCTTGCCGCTCGTATCTTTATG GTCGCGATTGAAGAAGCCAACGGTAAACACGTAGGTTTGACGGACATGATGGTTCGTTGGGCC AATGAAGACCCATACTTGGCACCGAAGCATGGTTACAAAGGCGAAACGCCAAGTGACCTTGGTT TTGATGCGAAGTACCACGTAGATCTAGGTGAGCATTACGCTGATTTCAAACAGTGGTTAGAAAC GTCCCAGTCGAACGGGTTGTTGAGTAAAGCGACGTTGGATGAATCCACTAAAACGGTTCATCTT GGCTATAGCTATCAAGAACTTCAGGATTTGACGGGTGCTGAATCGGTGCAAATGGCGTTCTACT TCCTGAAAGAAGCGGCGAAGAAAGCGGATCCGATTTCTGGTGATTCAGCTGAAATGATACTGCT GAAGAAATTTGCAGATCAAAGCTACTTATCTCAACTTGATTCCGACCGAATGGATCAAATTGAAG GTATCTACCGCAGTAGCCATGAGACGGATATTGACGCTTGGGATCGTCGTTACTCTGGTACAGG CTATGATGAGCTGACGAATAAGCTTGCTAGTGCAACGGGCGTTGACGAGCAGCTTGCGGTTCTT CTGGATGATCGTAAAGGCCTCTTGATTGGTGAAGTGCATGGCAGCGACGTCAACGGCCTACGC TTTGTTAATGAACAGATGGATGCACTGAAAAAACAGGGAGTCACAGTCATTGGCCTTGAGCATTT ACGCTCAGACCTTGCGCAACCGCTGATTGATCGCTACCTAGCTACGGGTGTGATGTCGAGTGA ACTAAGCGCAATGCTGAAAACAAAGCATCTCGATGTCACTCTTTTTGAAAACGCACGTGCTAACG GTATGCGCATCGTCGCGCTGGATGCAAACAGCTCTGCGCGTCCAAATGTTCAGGGAACAGAAC ATGGTCTGATGTACCGTGCTGGTGCTGCGAACAACATTGCGGTGGAAGTATTACAAAATCTGCC TGATGGCGAAAAGTTCGTTGCTATCTACGGTAAAGCGCATTTGCAGTCTCACAAAGGGATTGAA GGGTTCGTTCCTGGTATCACGGCGCGTCTCGATCTTCCTGCGCTTAAAGTCAGTGACTCGAACC AGTTCACAGTTGAACAAGACGATGTAAGTCTACGTGTTGTCTACGATGATGTTGCTAACAAACCG AAGATCACGTTCAAGGGCAGTTTGTAG
rrsp-mRNA – no tag	ATGGGTGATAAAACCAAGGTCGTGGTCGATTTAGCGCAAATCTTTACGGTGCAAGAGCTGAAAG AAAGAGCAAAAGTTTTTGCTAAACCGATTGGCGCATCCTACCAAGGTATTCTCGATCAACTCGAC CTTGTGCATCAGGCTAAAGGCCGCGATCAAATCGCAGCGAGCTTTGAGCTTAATAAGAAGATTA ATGACTACATCGCTGAACATCCAACTTCGGGGCGTAATCAAGCGCTAACGCAGTTGAAAGAGCA GGTCACCAGTGCGTTGTTTATCGGTAAGATGCAAGTTGCCCAAGCGGGTATTGATGCAATCGCA CAAACAAGACCGGAGCTTGCCGCTCGTATCTTTATGGTCGCGATTGAAGAAGCCAACGGTAAAC ACGTAGGTTTGACGGACATGATGGTTCGTTGGGCCAATGAAGACCCATACTTGGCACCGAAGC ATGGTTACAAAGGCGAAACGCCAAGTGACCTTGGTTTTGATGCGAAGTACCACGTAGATCTAGG TGAGCATTACGCTGATTTCAAACAGTGGTTAGAAACGTCCCAGTCGAACGGGTTGTTGAGTAAA GCGACGTTGGATGAATCCACTAAAACGGTTCATCTTGGCTATAGCTATCAAGAACTTCAGGATTT GACGGGTGCTGAATCGGTGCAAATGGCGTTCTACTTCCTGAAAGAAGCGGCGAAGAAAGCGGA TCCGATTTCTGGTGATTCAGCTGAAATGATACTGCTGAAGAAATTTGCAGATCAAAGCTACTTAT CTCAACTTGATTCCGACCGAATGGATCAAATTGAAGGTATCTACCGCAGTAGCCATGAGACGGA TATTGACGCTTGGGATCGTCGTTACTCTGGTACAGGCTATGATGAGCTGACGAATAAGCTTGCT AGTGCAACGGGCGTTGACGAGCAGCTTGCGGTTCTTCTGGATGATCGTAAAGGCCTCTTGATTG GTGAAGTGCATGGCAGCGACGTCAACGGCCTACGCTTTGTTAATGAACAGATGGATGCACTGAA AAAACAGGGAGTCACAGTCATTGGCCTTGAGCATTTACGCTCAGACCTTGCGCAACCGCTGATT GATCGCTACCTAGCTACGGGTGTGATGTCGAGTGAACTAAGCGCAATGCTGAAAACAAAGCATC TCGATGTCACTCTTTTTGAAAACGCACGTGCTAACGGTATGCGCATCGTCGCGCTGGATGCAAA

	CAGCTCTGCGCGTCCAAATGTTCAGGGAACAGAACATGGTCTGATGTACCGTGCTGGTGCTGC GAACAACATTGCGGTGGAAGTATTACAAAATCTGCCTGATGGCGAAAAGTTCGTTGCTATCTAC GGTAAAGCGCATTTGCAGTCTCACAAAGGGATTGAAGGGTTCGTTCCTGGTATCACGCACCGTC TCGATCTTCCTGCGCTTAAAGTCAGTGACTCGAACCAGTTCACAGTTGAACAAGACGATGTAAG TCTACGTGTTGTCTACGATGATGTTGCTAACAAACCGAAGATCACGTTCAAGGGCAGTTTGTAG

822

823